Physics – Uspekhi **37** (12) 1187 – 1212 (1994)

CONFERENCES AND SYMPOSIA

PACS numbers: 01.10.Fv

P L Kapitza Centenary International Symposium at the P L Kapitza Institute for Physical Problems (Moscow, 22 – 23 June 1994)

The P L Kapitza Centenary International Symposium held on 22 – 23 June 1994 at the P L Kapitza Institute of Physical Problems of the Russian Academy of Sciences, celebrated the centenary of P L Kapitza's birth.

The following reports were presented at the symposium:

(1) **A F Andreev** (P L Kapitza Institute, Russia) "New quantum states in helium crystals"

(2) **H E Hall** (University of Manchester, UK) "Mechanical experiments in superfluid helium"

(3) **M Krusius** (Helsinki University of Technology, Finland) "Rotated superfluid ^{3}He"

(4) **E J-A Varoquaux** (Universite Paris-Sud, France) "Phase slippage in superfluids"

(5) **G R Pickett** (University of Lancaster, UK) "Excitations in superfluid ^{3}He"

(6) **D M Lee** (Cornell University, USA) "Identical spin rotation effects in quantum fluids"

(7) **I A Fomin** (P L Kapitza Institute, Russia) "Spin currents in superfluid and normal Fermi liquids"

(8) **O V Lounmasmaa** (Helsinki University of Technology, Finland) "Nuclei in silver and rhodium metals at positive and negative nanokelvin temperatures"

(9) **G Frossati** (University of Leiden, The Netherlands) "A fourth-generation cryogenic gravitational antenna"

(10) **M Date** (Japan Atomic Energy Research Institute, Japan) "Recent progress in high field magnetism"

(11) **B P Zakharchenya** (A F Ioffe Institute, Russia) "Quasiparticles – excitons in strong magnetic fields and gemini recombination"

(12) **A S Levitov** (L D Landau Institute, Russia) "Aharonov – Bohm effect in mesoscopic conductors"

(13) **F Pobell** (University of Bayreuth, Germany) "Acoustic properties of glasses and polycrystals at very low temperatures"

(14) **J T M Walraven** (University of Amsterdam, the Netherlands) "The Kapitza leap on the boundary of superfluid ^{4}He and atomic hydrogen gas"

The authors' own extended summaries of some reports, and the full text of those of G F Frossati and M Date, are presented below. The contributions were submitted in English and are reproduced largely as supplied.

Uspekhi Fizicheskikh Nauk **164** (12) 1277 – 1302 (1994)
Submitted in English by the authors

PACS numbers: 67.80.–s

New quantum states in helium crystals

A F Andreev

The name of Petr Leonidovich Kapitza ranks very highly among the outstanding scientists of the world not only in physics, especially the physics and technique of low temperatures and strong magnetic fields. Nevertheless, when discuss-ing topics of present symposium, the organising committee decided to pay primary attention to the above mentioned sections of physics, where Kapitza's contribution is particularly valuable. Our intention was to invite those scientists from different countries, who work in these fields most actively. It is no surprise that many participants turn out to be closely connected with the Kapitza Institute for Physical Problems. This Institute of Russian Academy of Sciences was indeed a beloved creation of our hero of this anniversary. So this Centenary International Symposium is not only a tribute of respect of the world scientific community to the memory of a great colleague, but also a practical discussion of the current state of an area that has been founded and developed owing to the outstanding works of Kapitza.

The physics of quantum helium crystals is based on ideas of the physics of quantum liquids, essentially developed in the works of P Kapitza and L Landau. These crystals are characterised by the anomalously large amplitude of particle zero-point oscillations. Essential quantum delocalisation in crystals is connected with this amplitude. Not only crystal particles, but, in general, any point defects are delocalised in crystal lattice because of quantum tunnelling. From this fact we can infer some simple but quite general ideas that show the possibility of realising a number of new quantum states with unusual 'super' properties in helium crystals.

Here is the general idea [1]. Let us consider classical crystal with point defects of definite type. This system is disordered, because crystal defects are randomly distributed. Because of the quantum delocalisation, every point defect is uniformly 'spread' over the crystal volume. So we get ideally a periodical crystal with specific properties, depending on the character of quantum delocalised point defects.

Here are the most interesting examples:

1. Vacancies

A quantum crystal, with finite concentration of vacancies at sufficiently low temperatures (zero-point vacancies), should possess many unusual properties, including superfluidity [1]. Current experimental data [2 – 4] do not allow

us to prove conclusively the existence of the discussed quantum states in ^{4}He or ^{3}He crystals.

2. Isotopic impurities

The phenomenon of quantum diffusion is due to quantum delocalisation of ^{3}He impurities in ^{4}He crystals [5]. Fermi degeneration [6] of He impurities was observed in two-dimensional ^{4}He crystals. These impurities behave as quasiparticles with an effective mass roughly equal to twenty masses of the helium atom. They are the heaviest of known fermions.

3. Dislocation loops

Equilibrium plasticity [7] is a new property of a quantum crystal with delocalised topological defects (dislocation loop type). In this case the crystal shape is changed at thermodynamic equilibrium while the shape of elementary cells of the crystal remains the same. An experimental study of this effect may help to understand the nature of the 'elementary carrier' of plasticity.

4. Surface defects

Quantum delocalisation of defects on helium crystal surface (steps and kinks) causes the effect of super-crystallisation. It manifests itself as crystallisation waves [8, 9]. Now these waves are used [10] as a very effective method of investigating the thermodynamic and kinetic properties of crystalline surfaces. At ultralow temperatures (100 μK and less) peculiar magnetic crystallisation waves [11] should be observed.

References

1. Andreev A F , Lifshitz E M *Zh. Eksp. Teor. Fiz.* **56** 2057 (1969)
2. Wiegers S A J, Kranenburg C C, Jochemsen R, Vermeulen G A, Bedell K S, Frossati G *Jpn. J. Appl. Phys.* **26** CJ26 (1987)
3. Van de Haar P G, van Woerkens C M, Meisel M W, Frossati G *J. Low Temp. Phys.* **86** 349 (1992)
4. Lengua G A, Goodkind J M *J. Low Temp. Phys.* **79** 251 (1990)
5. Andreev A F "Quantum Crystals" in *Progress in Low Temperature Physics* Vol. 8 (Ed. D F Brewer) (Amsterdam: North Holland, 1982)
6. Saunders J, Mikheev V A, Lusher C P, Cowan B P *Phys. Rev. Lett.* **69** 2807 (1992)
7. Andreev A F, Bazaliy Ya B, Savitchev A D *J. Low Temp. Phys.* **88** 101 (1991)
8. Andreev A F, Parshin A Ya *Zh. Eksp. Teor. Fiz.* **75** 1511 (1978)
9. Keshishev K O, Parshin A Ya, Babkin A V *Zh. Eksp. Teor. Fiz.* **80** 717 (1981)
10. Keshishev K O, Andreeva O A in *Excitations in 2D and 3D Quantum Fluids* (Eds A G F Wyatt, H J Lauter) (New York: Plenum, 1992), p. 387
11. Andreev A F *Pis'ma Zh. Eksp. Teor. Fiz.* **58** 740 (1993)

PACS numbers: 67.57.De; 67.57.Fg; 67.40.Vs

Mechanical experiments in superfluid helium

H E Hall

I was first attracted to mechanical experiments on liquid helium by Kapitza's ingenious series of experiments demonstrating the mechanical reaction associated with a flow of heat in He-II. Indeed, my own first experiment as a research student was a variation on this theme designed to demonstrate the contribution of the superfluid fraction to this reaction force.

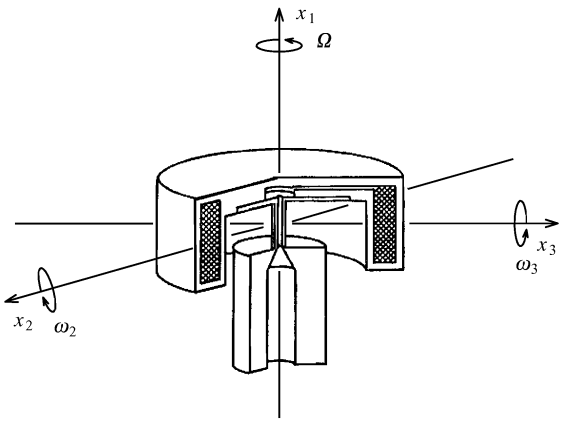

Figure 1. Combined torsion oscillator and gyroscope with alternating current.

By far the most fruitful in both ^{3}He and ^{4}He has been the development of the torsional oscillator and related devices, which originated with the pile of discs used by Andronikashili to measure the normal density. The main technical development of high precision devices of this type has come from John Reppy and his students at Cornell. A key early stage in this development was the invention by Reppy of the DC gyroscope as a nondestructive test for persistent currents in ^{4}He, which led to a truly fundamental experiment on the nature of superfluidity: the demonstration that as temperature is changed it is the velocity rather than the angular momentum of a persistent current that is conserved.

The current state of the art is illustrated in Fig. 1: the combined AC gyroscope and torsional oscillator built by Peter Gammel for experiments on persistent currents in superfluid ^{3}He. His thesis [1] gives a full discussion of the mechanics of this device and its design. Oscillation about the axis x_1 gives a conventional measurement of superfluid fraction. The near-degenerate modes about axes x_2 and x_3 are used to detect persistent angular momentum about axis x_1, via the gyroscopic coupling that it induces between them. Rotation of the cryostat about axis x_1 is used to set up persistent currents and also to calibrate the system via the Coriolis force. These experiments also showed that persistent currents had an effect on the textural dissipation associated with oscillation about axis x_1; this proved the most sensitive way of detecting persistent currents in the A-phase, which are much smaller than in the B-phase.

In the last few years Tim Bevan has developed at Manchester a novel mechanical device for investigating vortex mutual friction in rotating superfluid ^{3}He, shown in Fig. 2. In ^{4}He second sound was used for this purpose, but the small entropy and high viscosity of ^{3}He means that there is no such propagating mode. Instead, we make use of the high viscosity to clamp the normal fluid in two disc-shaped regions about 100 μm thick separated by a flexible Kapton diaphragm. When the diaphragm vibrates in the mode illustrated in Fig. 2, superfluid is forced to move as shown; this leads to vortex motion relative to the normal fluid and hence to mutual friction. The resistive component

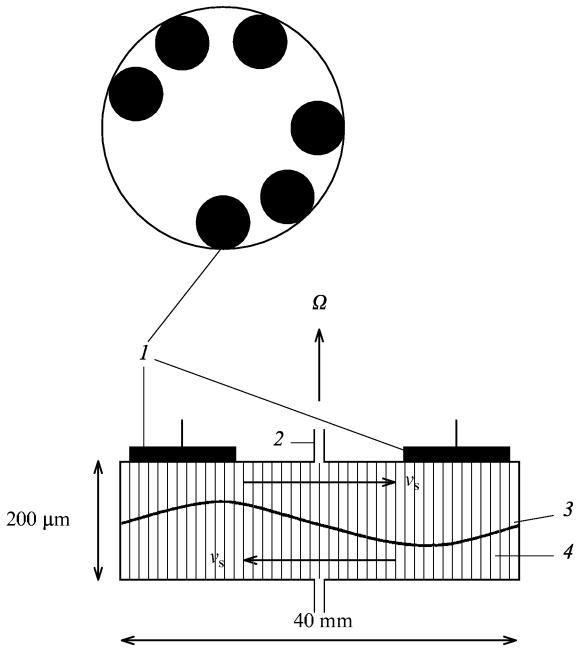

Figure 2. The pattern of device for measuring the mutual whirl friction in He: *1* — driving and detection electrodes, *2* — fill line, *3* — oscillating diaphragm, *4* — quantised whirl vortex.

of the force can be measured as a decrease in the Q of the diaphragm mode. But since there are two degenerate normal modes with orthogonal nodal lines, the reactive force perpendicular to $(v_s - v_n)$ can also be measured by the coupling it produces between these modes. Conceptually, the measurement of the reactive force is the same as the detection of persistent currents with the AC gyroscope. We have now obtained good-quality data on both components of mutual friction in the B-phase; the results are being published elsewhere [2]. The behaviour observed in the A-phase is so far markedly less reproducible; we suspect problems with variable textures, over which we do not yet have control.

References

1. Gammel P L, Ph. D. Thesis, Cornell (1987)
2. Bevan T D C, Manninen A J, Cook J B, Armstrong A J, Hook J R, Hall H E, submitted to *Phys. Rev. Lett.*

PACS numbers: 67.40.Hf

Phase slippage in superfluids

E J -A Varoquaux

1. Historical introduction

This talk describes recent experiments involving the flow of superfluids through apertures of submicron sizes and which have revealed the existence of the analogue of the DC-Josephson effect in superfluid ^{3}He and the occurrence of dissipative slippage of the quantum-mechanical phase in superfluid ^{4}He. A recent survey of this topic by O Avenel and the author can be found in Ref. [1].

The first study of superflow through channels of micron sizes was performed by P L Kapitza in 1937 [2] in a series of famous experiments in which he showed that, if superfluid ^{4}He had a viscosity, the viscosity coefficient would be smaller than 10^{-9} poise, i.e. smaller by four orders of magnitude than that of liquid hydrogen, the substance with the smallest coefficient of viscosity known previously. He coined the word 'superfluidity' to describe the remarkable property. His discovery led to the search of the mechanism which limits the velocity of the flowing superfluid and which fixes the critical threshold above which dissipation appears.

Since then, the problem of the critical velocity in superfluid ^{4}He has been given particular attention, first by L D Landau who set a limit for the maximum velocity at which the energy spectrum of the elementary excitations in the bulk superfluid remains well-behaved, and then by R Feynman, who realised that vortices played a major role in the appearance of dissipation in the superfluid flow through a channel. He gave a rough and intuitive argument by which he established the rate $\dot{n}$ at which vortices are formed at the outlet of the channel of typical size d. By requiring that the energy taken away by the vortex rings, formed with a size comparable to that of the aperture, be less than the kinetic energy brought by the flowing fluid, he obtained an estimate for the critical velocity. This estimate depends on the channel size but not on the temperature or the pressure, except very weakly through the dependence of the coherence length a_0. It gives a fair description of a wide class of critical velocity measurements, but not of the most recent ones, as shall be discussed below.

It can be noted that Feynman's derivation of the number of vortices emitted per unit time at the mouth of the orifice is nothing but the AC-Josephson formula which is usually written as

$$\hbar \frac{\partial \varphi}{\partial t} = -\mu ,$$

φ being the phase of the wavefunction and μ the chemical potential. In flows through apertures typical dimensions of which are of the order of the coherence length, it may also be expected that the DC-Josephson expression relating the current J to the phase difference $\delta\varphi$ across the aperture be valid. In the ideal case of a pure quantum tunnel effect, this expression reads:

$$J = J_c \sin \delta\varphi ,$$

where J_c is the maximum current that can flow without dissipation through the weak link. In less ideal junctions, such as micro-bridges for superconductors or micro-apertures for superfluids, the current–phase relation is not necessarily a sine function but it remains periodic by 2π in the phase difference. This stems, on heuristic grounds, from the fact that the phase of the wavefunction is defined modulo 2π.

2. Description of the experiment

Experiments were attempted as early as 1965 to verify the existence of Josephson-type effects in superfluid ^{4}He as they constitute an important step in the understanding of critical velocities for superflows, and, more generally, of the nature of superfluidity. After Richards and Anderson first reported the observation of frequency mixing features which they attributed to the AC-Josephson effect, a number of experiments were carried out to confirm this observation but failed to do so conclusively. It was then thought that Josephson-type effects were masked in

superfluids by the randomness intrinsically associated with the motion of vortices.

The discovery in 1972 by Osheroff, Richardson, and Lee of the superfluidity of ^{3}He revived the interest for these questions as the coherence length for Cooper-paired ^{3}He is two orders of magnitude larger than that for ^{4}He, which is of atomic dimension. It thus became possible to envisiage an experiment in which the micro-aperture would be an actual weak link and would provide a coupling between two superfluid baths of the required strength to observe genuine Josephson effects.

Such an experiment was attempted in a number of laboratories, including a joint effort by Centre National de la Recherche Scientifique and Commissariat de l'energie Atomique at Orsay and Saclay by Oliver Avenel and the author. A micro-aperture in the shape of a slit of 0.3×5 μm was milled with the help of a focused beam of gallium ions in a nickel foil of 0.2 μm in thickness. This micro-aperture was fitted to a Helmholtz resonator also equipped with a flexible membrane. This membrane, excited electrostatically, was used to drive the fluid in and out of the resonator. Its motion was monitored by electrodynamic means, a conventional rf-SQUID being used as amplifier to achieve a very high resolution. The natural resonance frequency of the resonator lies in the 1–30 Hz range and high-precision digital techniques are used for data acquisition and filtering. Membrane displacements of 5×10^{-3} Å can thus be resolved in a time of 20 ms. A second channel was put in parallel with the micro-aperture so that pressure and temperature equilibria can be reached more rapidly. But this also enabled persistent currents to be maintained in the loop threading the micro-aperture and the parallel channel. As such, this device is the direct hydrodynamic analogue of the superconducting rf-SQUID. Its operation can be very accurately modelled by numerical techniques on a computer.

3. The DC-Josephson effect in superfluid ^{3}He

After some early results in ^{4}He were obtained, and in particular the observation of staircase patterns in the amplitude versus drive response of the resonator which are typical of rf-SQUID operation, ^{3}He was put into the cell and cooled to submillikelvin temperatures. Staircase patterns similar to those in ^{4}He were also observed in ^{3}He indicating that similar nonlinear behaviour was taking place in the weak link, revealing the existence of a periodic current–phase relation with a period of 2π in the phase difference and obeying the AC-Josephson relation. For the weak link described above, the current–phase relation turned out to be close to a sine function at zero pressure and $T > 0.8T_c$ as expected. A near-ideal DC-Josephson effect was thus observed. Deviations from a pure sine function turn out to be primarily due to ideal fluid hydrodynamic effects at the inlet and outlet of the micro-aperture. Below $0.7T_c$, or at higher pressures, the coherence length becomes significantly smaller than the size of the aperture and the current–phase relation becomes more complicated, and even history dependent, which seems to indicate that textures may play a role. An interesting result is that the weak link behaviour appears to be the same irrespective of whether the A or B phase prevails in the bulk. This shows that the superfluid order parameter in the weak link is dominated by the proximity of the walls. Its precise structure, and the manner by which it is affected by textures in the bulk remain an interesting problem to be studied.

4. The case of ^{4}He

As briefly recalled above, the case of ^{4}He, in spite of numerous studies and most notably those conducted recently at the University of California at Berkeley and the University of Minnesota, is also far from being resolved, but it has already brought about a number of surprising and enlightening results. Although is appears quite certain that phase slips correspond to sudden jumps of the quantum-mechanical phase difference across the aperture by 2π, the threshold at which these slips occurs has been found to vary with temperature as $1 - T/T_0$, with $T_0 \simeq 2.45$ K, from about 1.9 K down to ~ 0.15 K. Below this temperature, it exhibits a sharp change of behaviour and becomes temperature independent. However, it still shows a weak dependence on pressure, decreasing by about 12% when the pressure is raised from 0 to 24 bar, and a very striking dependence on minute concentrations of ^{3}He in the 10^{-9} range, decreasing very sharply below a temperature which is found to depend logarithmically on impurity concentration. These observations conclusively show that the process by which new vortices are released in the aperture — nucleation, unpinning, etc. — involve very small energies, of the order of a few kelvin. Furthermore, the temperature dependence implies that the process is thermally assisted above 0.15 K. By the same token, it should exhibit fluctuations, which are indeed observed, with the correct temperature dependence. The plateau below 0.15 K is interpreted as being due to quantum tunnelling, when the zero-point fluctuations of the various (phonon) modes constituting the thermal bath finally take over thermal excitations at sufficiently low temperatures.

These findings can be explained by assuming that very small half-rings are nucleated at certain sites, located where the superfluid velocity is the highest, at some asperity in the immediate vicinity of some sharp bend of the wall of the aperture. Such a point of view has already been taken by G Volovik (1972), E B Sonin (1982), and Muirhead–Vinen–Donnelly (1984). The problem can be solved nearly exactly and the energy barrier opposing nucleation $E_a(v_s)$ can be evaluated as a function of the superfluid velocity v_s. The nucleation rate follows if one further makes use of a result established originally by V I Goldanskii (1959) and later independently by I Affleck (1981) relating the attempt frequency $\omega_0/2\pi$ to the cross-over temperature T_q between the thermal and quantum regimes:

$$\hbar\omega_0 = 2\pi k_B T_q \ .$$

The nucleation rate, and hence the most probable values of the observable quantities in the problem can thus be computed by carrying these steps in succession with only one parameter which is not strictly determined, namely the core parameter a_0 of a very small vortex lying very close to a wall. Comparing the outcome of the calculation to the experimental results fixes a_0 at approximately 5 Å.

The effect of ^{3}He on the critical velocity for phase slips is also very interesting to study as it provides a way to evaluate the superfluid velocity at the nucleation site which cannot be measured directly. Detailed measurements of the critical velocity as a function of temperature at the low-temperature end of the quantum plateau for impurity concentrations ranging from 0.9×10^{-9} to 10^{-7} have led

to a value of the local superfluid velocity at the nucleation site in our aperture of 22 m s^{-1}, a value compatible with that for a_0 of 5 Å.

Thus a picture emerges for the mechanism of 2π phase slip: (1) nucleation event takes place when the appropriate conditions are met, (2) the newly formed microscopic vortex moves in the superfluid flow field according to the law of ideal fluid mechanics, at least as long as normal fluid friction can be neglected. It grows in size in the diverging flow field converting kinetic energy from the potential flow field into vortical line energy and traverses all the streamlines threading the aperture. Thus, the quantum mechanical phase experiences a change by 2π on every possible path going from one side of the aperture to the other, leading to an overall reduction by 2π of the total phase winding number across the aperture.

This scenario accounts for the properties of phase slips by 2π and for the temperature dependent (above 0.15 K), orifice-size independent critical velocity associated with them. Other events, involving slips of the phase by multiples of 2π and occurring at velocities which can be smaller than the nucleation critical velocity for 2π phase slips are also observed for larger orifices, and also for higher Helmholtz resonance frequencies. These events, which are currently investigated, are not described by the preceding mechanisms and may provide a route from the nucleation regime to the more commonly met critical velocity of the Feynman type.

References

1. Avenel O, Varoquaux E J-A *Physica B* **197** 306 (1994)
2. Kapitza P L *Nature (London)* Jan. 8 (1938)

PACS numbers: 67.57.–z; 67.57.Lm

Spin currents in superfluid and normal Fermi liquids

I A Fomin

The superfluidity of helium, discovered by P L Kapitza in 1937, became one of the central problems in condensed matter physics again at the beginning of seventies. The reason was the discovery of superfluid phases of the helium lighter isotope—^{3}He. Unlike ^{4}He, atoms of ^{3}He are fermions; therefore in this case superfluidity, in superconductors, originates from Cooper pairing effect. This occurs at much lower temperatures than for ^{4}He—around 1 mK.

What is essentially new here is that for ^{3}He Cooper pairs have spin equal to 1, compared with ordinary superconductors. This distinction generates a number of nontrivial properties: for example, a condensate of such pairs can transfer spin current that is not connected with mass flow.

At the pairing with a nonzero spin, Fermi liquid symmetry, related to rotations of all spins through arbitrary angle, gets broken. Hence, the ground state is degenerate with respect to three continuous parameters (for example, Euler angles), determining such rotation. Strict degeneracy takes place when these angles are constant in space. There are, however, states, close to the ground state, in which angles of rotation are slowly changing in space. Currents, transferring spin components, conjugated with corresponding angles, flow in such states. These currents tend to restore uniformity of condensate, but not thermodynamic equilibrium; their contribution to spin transfer is reversible. Usually they are called superfluid spin currents, in order to distinguish them from quasiparticle spin transfer, which is also possible in normal phase. At the Kapitza Institute for Physical Problems A S Borovik-Romanov, Yu M Bun'kov, V V Dmitriev and Yu M Mukharskii have made experiments resulting in finding phenomena that owe their existence to spin currents. Their results are reviewed in the first part of this report along with the author's theoretical approaches.

A typical manifestation of ^{4}He superfluidity is a thermomechanical effect, i.e. an unusually strong reaction to temperature nonuniformity. Similarly, spin superfluidity causes anomalous reaction of ^{3}He to magnetic field nonuniformity. In nuclear magnetic resonance experiments nonuniformity of the magnetic field leads to rising spin precession phase difference in time at different points of the helium's volume. This difference is similar to the phase difference of the ^{4}He condensate wave function; it generates spin currents, which redistribute spin over the helium volume. If the volume is closed, then such a redistribution in the B-phase of ^{3}He creates a structure consisting of two domains [1–3]. In the domain located in relatively stronger magnetic fields, magnetisation has the equilibrium value; in the other domain it deviates from the equilibrium direction. The angle of deviation equals $\arccos(-1/4)$. The whole structure precesses with the same frequency, which is equal to the local Larmor frequency in the site, where the wall separating two domains is situated. Under conditions of pulse nuclear magnetic resonance the wall position is determined by the conservation of the projection of full magnetisation on the direction of magnetic field. Absence of spin currents in stationary states gives a constant precession phase throughout the precessing domain. This allows one to call it 'uniformly precessing domain'. Brought-in phase precession takes place in spite of nonuniformity of magnetic field; such precession is being observed until relaxation of the whole structure takes place. A brought-in phase precession gives rise to extremely long-living signal of induction in nuclear magnetic resonance experiments with B-phase. Separation of uniform precession into domains in ^{3}He–B was confirmed by direct experiments.

Relaxation of a two-domain structure towards equilibrium proceeds through enlargement of the equilibrium domain at the expense of the precessing one, while the domain wall moves in the direction of weaker fields. Energy losses may be compensated by means of resonance high-frequency field, the same as is done when using continuous nuclear magnetic resonance. In this way brought-in phase precession can be maintained indefinitely long. This method allowed the above mentioned group of scientists from the Kapitza Institute to observe also stationary spin flowing through the channel between two ^{3}He volumes, while the brought-in phase precession was maintained in both volumes [4]. Induced current went up with increasing precession phase difference in the two volumes, until it reached a critical value. When the channel length and diameter decreased to the dimensions of the effective coherence length, one could observe the transition to Josephson effect for spin current: it became a continuous

periodic function of phase difference [5]. Two-domain structure is analogous to a two-phase system separated in an external field. There are surface and volume modes of oscillation in a system like that [6]. Surface oscillations are similar to gravity waves of a liquid surface in a gravitational field. The square-root dependence of frequency on wave vector also resembles the gravitational case. Precession phase degeneracy gives rise to a volume gapless mode. Both types of oscillations were observed [7].

The effects, characteristic for superfluids, may, under some conditions, be observed also in normal liquids. According to A F Andreev [8], one can observe thermo-mechanical effect in ^{4}He beyond the lambda point. The same is true for ^{3}He. Recently three groups — in Japan (Osaka) [9], in USA (Cornell) [10], and in Russia (Kapitza Institute) [11] in different experiments discovered anomalies indicative of the existence of coherently precessing spin structure also in solutions of ^{3}He in ^{4}He, where dissolved ^{3}He behaves as normal Fermi liquid. Anomalies were observed at temperatures near and below 1 mK, i.e. in collisionless region. Here, according to Leggett [12], Fermi liquid interaction gives rise to a nondissipative component of spin current. Theoretical and numerical analysis of spin dynamics equations for normal Fermi liquid has shown [13] that, owing to this component, in a weakly nonuniform magnetic field, in a normal Fermi liquid, under conditions of pulse nuclear magnetic resonance, coherently precessing spin structure is formed, also consisting of two domains. In one domain magnetisation is parallel; in the other, anti-parallel to the field. From this analysis it follows that a similar structure can arise in liquid ^{3}He above the temperature of transition to the superfluid state, as well as in normal metals, were Fermi liquid consists of conduction electrons. Future investigations of spin currents and coherently precessing spin structures will lead to better understanding of the properties of interacting Fermi liquids, both superfluid and normal.

References

1. Borovik-Romanov A S, Bun'kov Yu M, Dmitriev V V, Mukharskii Yu M *Pis'ma Zh. Eksp. Teor. Fiz.* **40** 256 (1984)
2. Borovik-Romanov A S, Bun'kov Yu M, Dmitriev V V, Mukharskii Yu M, Flachbart K *Zh. Eksp. Teor. Fiz.* **88** 2022 (1985)
3. Fomin I A *Pis'ma Zh. Eksp. Teor. Fiz.* **40** 260 (1984); *Zh. Eksp. Teor. Fiz.* **88** 2039 (1985)
4. Borovik-Romanov A S, Bun'kov Yu M, Dmitriev V V, Mukharskii Yu M *Pis'ma Zh. Eksp. Teor. Fiz.*. **45** 68 (1987)
5. Borovik-Romanov A S, Bun'kov Yu M, de Waard A, Dmitriev V V, Makrotsieva V, Mukharskii Yu M, Sergatskov D A *Pis'ma Zh. Eksp. Teor. Fiz.* **47** 400 (1988)
6. Fomin I A *Pis'ma Zh. Eksp. Teor. Fiz.* **43** 134 (1986)
7. Bun'kov Yu M, Dmitriev V V, Mukharskii Yu M *Pis'ma Zh. Eksp. Teor. Fiz.* **45** 131 (1986)
8. Andreev A F *Zh. Eksp. Teor. Fiz.* **59** 1819 (1970)
9. Akimoto H, Ishikawa O, Gong-Hun oh, Nakagawa M, Hata T, Kodama T *J. Low. Temp. Phys.* **82** 295 (1991)
10. Nunes G (Jr), Jin C, Hawthorne D L, Putnam A M, Lee D M *Phys. Rev. B* **46** 9082 (1992)
11. Dmitriev V V, Moroz V V, Vysotskii A S, Zakazov S R (in press)
12. Leggett A J *J. Phys. C* **3** 448 (1970)
13. Dmitriev V V, Fomin I A *Pis'ma Zh. Eksp. Fiz.* **59** 352 (1994)

PACS numbers: 04.80.Nn; 95.55.Ym

A fourth-generation cryogenic gravitational antenna

G Frossati

Abstract. Large metallic cylinders with a mass of several tons have been cooled to liquid helium temperatures and recently down to T $\sim$ 100 mK leading to the most sensitive gravitational wave detector (NAUTILUS). The sensitivity is still not enough to detect waves from distances so large that the number of events becomes several per year. Cooling spherical detectors with a mass around 100 tons to temperatures around 10 mK could achieve this goal giving rise to a new astronomy.

Introduction

Gravitational waves were predicted by Einstein in 1916, in the framework of his General Theory of Relativity, but they have never been detected despite intensive efforts of many experimental groups in the last 30 years [1]. One of the reasons is that only accelerated masses possessing a quadrupole moment can give rise to g-waves since the time derivative of the dipole moment $\boldsymbol{d} = \sum_i m_i \boldsymbol{x}_i$, (where i labels the particle of mass m_i and position $\boldsymbol{x}_i$) represents the total momentum of the system, which is conserved. The power radiated has thus a term in $1/c^5$ instead of $1/c^3$ as for electromagnetic waves. As an example [1], a cylindrical steel bar of 1000 tons, 100 m long rotating at the largest possible speed before breaking ($\omega = 20$ rad s^{-1}) around an axis perpendicular to the axis of the cylinder would emit 10^{-26} W. This is an extremely small value, but could still be detected, eventually, if we had a detector which could absorb all the energy emitted. Unfortunately the cross section of even the best detectors is extremely small. For those acquainted with low-temperature problems this is easy to see this since it is analogous to the Kapitza resistance problem. In fact, Einstein's equations are similar to the equations of elasticity in common materials, except that the spring constant $c^4/8\pi G$ has dimensions of force/length. Here G is the gravitational constant $G = (6.6720 \pm 0.0041) \times 10^{-11}$ m^3 s^{-2} kg^{-1} and c is the speed of light. As D Blair discusses in his book [1], the space–time continuum can be seen as an extremely rigid elastic body (since the 'elastic constant' is of order 10^{43} N), where the g-waves are like sound waves propagating at the speed of light. The characteristic impedance of a solid to a sound wave $\rho V/\sigma$ (where σ is the area facing the wave), can be assimilated to c^3/G for space–time. For liquid helium and copper, the ratio of the impedances is $(\rho V)_{\mathrm{Cu}}/(\rho V)_{\mathrm{He}} \cong 1.8 \times 10^3$, while that between space–time and copper is of the order of 10^{28}, which means that g-waves travel unimpeded through ordinary matter. Transferring energy from these high-velocity 'phonons' to a massive antenna is thus very inefficient, the cross section being $\Sigma_0 = 0.68 G v^2 M/\pi c^3$ (for a wave coming in the optimum direction [2]) where v is the speed of sound in the detector material and M is the mass of the detector. The cross section of present detectors, with masses around 2 tons, and sound velocities of order 5 km s^{-1} is thus limited to about 10^{-25}. Supposing we have a detector of that size tuned to our rotating bar, the energy absorbed would be of order $10^{-25} \times 10^{-26} = 10^{-51}$ W which is

ridiculously small, corresponding to the power absorbed in the detector due to one (3 Hz) quantum every 10^{11} years!

For the above reason only gravitational waves of cosmic origin like supernovas, coalescence of double stars, trapping of stars by black holes, etc., are candidates for emitting gravitational waves detectable on earth. The frequency of such events is very low in our galaxy. Supernovas are expected every 30–40 years while binary coalescence might happen once every 1 000 000 years. If a large black hole exists at the centre of the galaxy it might trap a star every 1000 years [3]. We see that much larger volumes of space must be explored if gravitational waves are to be detected. Events from the large Virgo cluster situated at 10–20 Mpc (1 Mpc $\sim$ 3.6 million light-years) which has about 2500 galaxies are the preferred target, since there should be several events per year.

Two types of antennae have been developed in the last 20 – 30 years. The Weber antenna and the laser interferometer antenna [1]. Both use the fact that g.w. deform the metric tensor h so that matter interacting with the wave is subject to strain in the direction perpendicular to the propagation of the wave. Such strain $h = \Delta L/L$ is very small due to the small interaction cross section of the wave with matter. A supernova collapse in the centre of our galaxy (10 kpc) with 0.1% of one solar mass being converted in gravitational waves should produce a strain $h \cong 10^{-18}$ on Earth.

The interferometer antennae use very long-arm interferometers with relatively heavy mirrors reflecting laser light which goes back and forth many times so as to produce a very long effective L. Such antennae have great potential sensitivity but for the moment are still two orders of magnitude less sensitive than Weber antennae.

The Weber antennae [4] are made of high quality-factor materials (Q is typically several million) suspended so as to damp as much as possible the external vibrations at the resonant frequency. Nowadays the bars are cooled to decrease the Brownian noise. When the wave passes through the antenna, typically in a few milliseconds, it induces a (quadrupole) vibration which lasts for a time of the order of Q/ω. The vibration energy is transferred to a detector, typically a much smaller mass (or masses) attached and tuned to the bar frequency which thus vibrates with a much larger amplitude. This motion is detected in many ways, one of the best being capacitively. One of the electrodes of the capacitor, for instance, is a small mass transducer, with the larger displacement amplitude, while the other moves with the same amplitude as the bar. The capacitor is charged and the modulated voltage signal is detected with a state-of-the-art superconductive quantum interference device (SQUID). Other types of transducers are in use throughout the world, with various advantages and disadvantages. The resonance frequency of the bar is chosen to be the most probable for the predicted wave, typically a pulse of increasing frequency with most of the energy being emitted in milliseconds at a few hundred to a few thousand hertz [1, 2, 3].

The need for low temperatures in such gravitational wave detectors was clear since the 60s, when Weber operated a separated pair of room-temperature g.w. antennas in coincidence. In fact the ultimate sensitivity which can be achieved with a resonant-mass g.w. antenna can be written in terms of the energy spectral density $f(\nu_0)$ of the g.w. burst:

$$f(\nu_0) > \Sigma_0^{-1}\left(\frac{kT}{\beta Q} + 2kT_n\right) . \quad (1)$$

The mass is resonant at ν_0 with quality factor Q and temperature T. It is assumed that the motion is detected by a transducer whose electrical energy is a fraction β of the total antenna energy and is amplified with an electronic device of noise temperature T_n. Most groups throughout the world use cylindrical bars made of the high-Q aluminium alloy Al 5056 ($v_s = 5.1 \times 10^3$ m s^{-1}), whose length, of about 3 m, is fixed so as to resonate at a frequency ω_0 around 1 kHz, where the signal spectral energy density is expected to be largest. The typical mass is a few tons.

In Eqn (1) the first term on the right represents the noise due to the thermal fluctuation in the antenna (Brownian noise). The rate of fluctuation is related to coupling between the fundamental mode and the thermal reservoir. This coupling itself determines the acoustic loss of the bar. Thus the effective noise energy decreases as the relaxation time τ (or the quality factor Q) increases. The discovery that at low temperature it is possible to take advantage of the steep increase of the quality factor Q for aluminium alloys [5, 6] convinced most of the experimental groups to use this material.

The second noise term in Eqn (1) stems from the measurement process itself. It is due to the electronic noise of the transducer and amplifier. This noise has the familiar Nyquist form as experienced in most areas of electronic instrumentation. Josephson effect SQUID amplifiers, whose noise temperature can in principle approach the quantum limit ($T_n = h\nu/k = 47 \times 10^{-9}$ K at 1 kHz), are fundamental to g.w. antennae.

One can classify the different generations of Weber antennae by their thermodynamic temperature. The room temperature antennae developed by Weber in the 60s are said to be of the first generation. The 4.2 K cryogenic detectors developed in the 70s and operational in the 80s are of the second generation. In 1986 three such cryogenic detectors (Rome, LSU, Stanford) have set a new upper limit on the intensity of the g.w. reaching the Earth [7]. In 1989 the Rome antenna Explorer, cooled at 2 K with superfluid helium, reached the sensitivity of $h \cong 7 \times 10^{-19}$ [8].

Antennae operating below 1 K

In order to further reduce the effective temperature of the antennae, striving to reach the quantum limit of sensitivity it was suggested by W Fairbanks and his group that they be cooled to millikelvin temperatures. They considered cooling the antenna to 2 mK using electronic demagnetisation of the well-known paramagnetic salt CMN (cerium magnesium nitrate) [9]. This was never done and it is only with the development of powerful dilution refrigerators that cooling tons of metal became possible. The first group to succeed was the Rome group with their NAUTILUS antenna [10]. They demonstrated for the first time that a 2.3 ton mass can be cooled to below 100 mK. It will soon be followed by the AURIGA detector at the LNL (INFN-Legnaro) and the Stanford University detector. These antennae belong to the third generation.

Potentially NAUTILUS could reach a sensitivity of 3×10^{-21} when cooled to 30 mK with a SQUID amplifier working at the quantum noise limit. The strain on Earth

caused by an event in the Virgo cluster with 0.1% of a solar mass being converted into a gravitational wave pulse is $\simeq 2 \times 10^{-21}$, corresponding to an energy density at 1 kHz $f(\nu_0) = 3 \times 10^{-6}$ J m^{-2} Hz^{-1}. The cross-section of NAUTILUS for the best possible wave orientation is $\Sigma_0 = 8.44 \times 10^{-25}$ m^2 Hz. If one averages over all polarisations and over all directions the cross-section is decreased by a factor about 7.5. The energy absorbed in the antenna, given by $f(\nu_0)\Sigma_0$ is only 3.4×10^{-31} J which is less than one quantum at 1 kHz. Further increase in sensitivity requires quantum nondemolition techniques, now under study [11].

Spherical detectors (fourth-generation Weber detectors)

Spherical detectors could improve on resonant-mass bar detectors, even with the noise level unchanged.

It was recognised long ago by R Forward [12] that a spherical detector can be considered a true g.w. observatory. A free elastic sphere has 5 degenerate quadrupole modes of vibration that interact strongly with a g.w. A cylindrical bar has only one mode. Each mode can act as a separate antenna oriented towards a different polarisation and direction. The source direction and wave polarisations can be determined from the amplitudes of the quadrupole modes of the sphere. Moreover, comparing a sphere to a cylindrical bar of the same material and same resonant frequency (this conditions is roughly given by the equality: length of the bar = diameter of the sphere), the sphere has a larger cross section because it has a larger mass and because it is omnidirectional [3]. For instance, an aluminium sphere resonating at 1 kHz like the NAUTILUS cylindrical bar, has a diameter of 3 m and a mass of almost 38 tons, a factor of 17 more than the typical bars. The cross section improves by the same factor with respect to the optimally oriented cylinder and about a factor of 100 if averaging over all directions.

Since the technical feasibility of reducing the noise and approaching the quantum limit appears independent of whether the detector is a bar or a sphere, the above improvement in cross section is reflected in the sensitivity. This means that if the sensitivity of a quantum-limited cylinder, optimally oriented, is $h = 3 \times 10^{-21}$, the sensitivity of the sphere is $h = 3 \times 10^{-22}$ whichever the source direction, since h is proportional to $M^{1/2}$. If instead of Al one were to use a heavier alloy like CuBe or CuAl with the sound velocity kept about the same, one could gain further a factor 1.7 in h, going to about 1.7×10^{-22} without having to rely on quantum-nondemolition techniques. A spherical detector can detect in a very natural way not only the tensorial waves (spin 2) predicted by general relativity, but also the scalar waves (spin 0) predicted by the other metric theories of gravitation, like the theory of Brans and Dicke [14], developed to incorporate Mach's principle in a relativistic theory of gravitation. The scalar radiation is not excluded by the upper limits imposed by solar systems experiments. This type of radiation could be emitted by time variations of the source monopole moment, like in the radial oscillations of vibrating neutron stars, and should be detected by monitoring the excitations of the monopole mode of the sphere.

These facts were ignored for many years, perhaps because a spherical resonator was not considered as practical and simple as a cylindrical bar. New facts give today to the experimentalists the necessary confidence to start such an ambitious project:

—the reliability reached by the cryogenic resonant antennas;

—the feasibility of the cooling to below 0.1 K of the new generation of resonant antennas, demonstrated by NAUTILUS;

—the feasibility of a nodal point suspension to support a large resonant mass [15];

—the determination of a clear method for the orientational deconvolution of the signal from a set of transducers coupled to a spherical resonant mass [16].

The problem remains of developing transducers with lower noise temperature (at present about 1 mK) and larger coupling β.

Cryogenics of large-mass g.w. detectors: the Nautilus

In 1971 Weber cooled for the first time a 1.5 ton aluminium cylinder to liquid helium temperatures and... "Immediately after cooling, a very large amount of noise was observed. Some of the excess noise appeared to be associated with internal structural relaxation of the cylinder. Some noise was due to acoustic coupling of the high intensity noise associated with the liquid nitrogen and helium system" [17]. These considerations reflected the difficulties of operating a g.w. antenna at low temperatures, demonstrated by the twenty years efforts of several researchers in four continents. The problem was that for the first time a high-Q resonant mass of several tons had to be cooled to 4.2 K or below, being free to move and isolated so well from the rest of the world as to allow the detection of a displacement of the order of $\Delta L \simeq 10^{-18}$ m.

In a low-temperature system for a g.w. antenna, cryogenics and acoustic isolation requirements are strictly connected; they can be summarised as follows:

(a) ensure many months of operation time, with rare and brief interruptions in the data taking for cryogenic maintenance;

(b) ensure a constant and uniform temperature of the antenna; a stationary gaussian distribution of the amplitude of the bar vibrations, in absence of signals, is an important condition for a reliable antenna;

(c) do not add extra mechanical noise, in order not to excite the vibrational modes at a detectable level;

(d) preserve the inherent high mechanical quality factor Q of the bar.

The peculiar problem of a cryogenic g.w. experiment is to put a large resonant mass at the same time in good thermal contact but in very poor mechanical contact with an effective and largely autonomous cooling source.

At 4.2 K the liquid helium bath surrounding the antenna vacuum chamber serves as heat sink and some helium exchange gas is used to thermalise the detector. The gas is then pumped out before the data taking. The antenna temperature remains at about 4.2 K as long as the vacuum chamber is completely surrounded by the liquid helium. It has been found that the mechanical noise produced by the evaporating liquid helium must be attenuated by a factor 10^{-7} (140 dB) so as not to disturb the detector. This attenuation is provided by the suspension system, which is carefully designed to act as an efficient mechanical filter.

As mentioned before, the only refrigerator able to maintain temperatures down to 10 mK continuously even in the presence of large thermal inputs is the ^{3}He $-^4$He dilution refrigerator (DR) [18]. The most powerful DRs in the range of 50 mK and below (down to 1.9 mK)

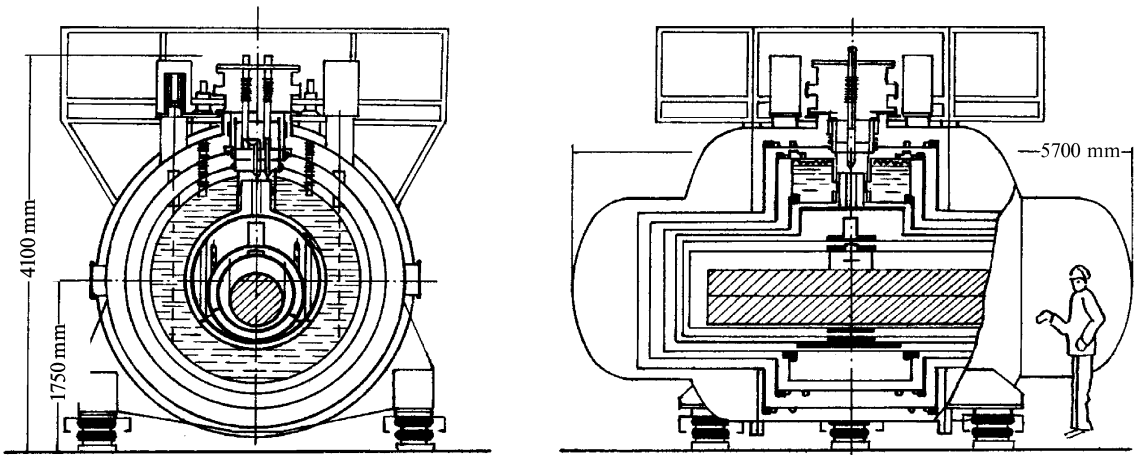

Figure 1. Layout of the NAUTILUS antenna.

have been built at the Kamerlingh Onnes Laboratory and can absorb 25 μW of heat applied outside the mixing chamber [19], at a temperature of 10 mK with circulation rates up to 10^{-2} mol s^{-1}.

Dilution refrigerators have been built with circulation rates of more than 1 mol s^{-1} [20] and very large cooling powers above 100 mK. DRs are themselves sources of noise so care must be taken to design them so as to minimise effects of turbulence and friction. One should use the minimum flow compatible with the heat leak on the antenna and shields. As the temperature decreases below 1 K, the most effective heat transfer mechanism between the antenna and the cooling source becomes the conduction by solid. This makes the mechanical isolation from the cooling source of an ultralow temperature antenna a much more difficult task than for an antenna at liquid helium temperature.

After a careful feasibility study [21], the first ultralow temperature detector NAUTILUS was constructed, assembled, and tested. The general layout of the cryogenic apparatus is shown in Fig. 1. The relevant feature of the cryostat is its central section, which is shorter than the cylindrical bar antenna (hereafter indicated as the bar) itself. This section contains two helium-gas-cooled shields, the liquid (He) reservoir (2000 litres of capacity), three OFHC copper massive rings and, through the top central access, a special $^3He-^4He$ dilution refrigerator [22]. End caps are fastened at each stage of the cryostat to complete the seven shields surrounding the bar. The shields are suspended to each other by means of titanium rods and constitute a cascade of low-pass mechanical filters. The overall mechanical vibration isolation at the bar resonant frequency (about 900 Hz) is of the order of −260 dB.

The first copper shield is thermally anchored to the 1 K pot of the refrigerator. The intermediate and inner shields are in thermal contact with two silver heat exchangers of the dilution refrigerator; the mixing chamber [23] cools the bar by means of an OFHC copper rod wrapped around the bar central section. The thermal path in the above cases is constituted by soft multiwire copper braids, in order to minimise the transmission of mechanical vibrations to the bar [24].

Fig. 2 shows the bar temperature during the cooling down. About three weeks were needed to reach 77 K, with the use of 8000 litres of liquid nitrogen, and about one week

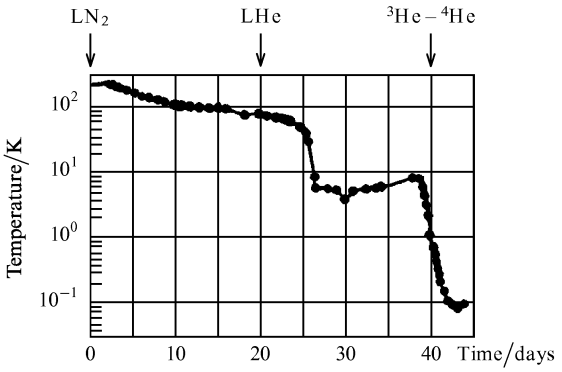

Figure 2. Temperature of the cylindrical bar vs time.

to achieve 4.2 K with the use of about 5000 litres of helium. The bar was kept at a temperature in the range 4.2 – 8 K for about two weeks, to perform various tests. Then the ultralow-temperature cooling was started. The initial temperatures of the bar and of the three copper shields were about 8 K. After filling the 1 K pot with He at low pressure, the mixture was condensed and circulated in the dilution refrigerator. After three days the calibrated Ge thermometers indicated a temperature of 95 mK on the bar end face and of 63 mK in the mixing chamber.

The observed features of the cooling agreed with an earlier model [25]. From the measured thermal gradient between the mixing chamber and the bar end (about 30 mK) an upper limit of 10 μW for the antenna heat leak (corresponding to 1.7 μW m^{-2}) was deduced. The overall helium evaporation rate was 50 litres day^{-1}.

The next step

Having acquired the recent experience with the NAUTILUS we are now considering the next step in g.w. detectors, that is, the spherical antenna. Since at least 6 transducers are required for the 5 resonant quadrupole modes and eventually a monopole mode, it is to be expected that the very high Q obtained with Al 5056 will be significantly reduced, possibly by a factor 2–3 per transducer. It seem thus better to look for alloys which could be cooled to lower temperatures so as to keep or decrease $T_{\text{eff}} = T/\beta Q$. Copper alloys are quite interesting,

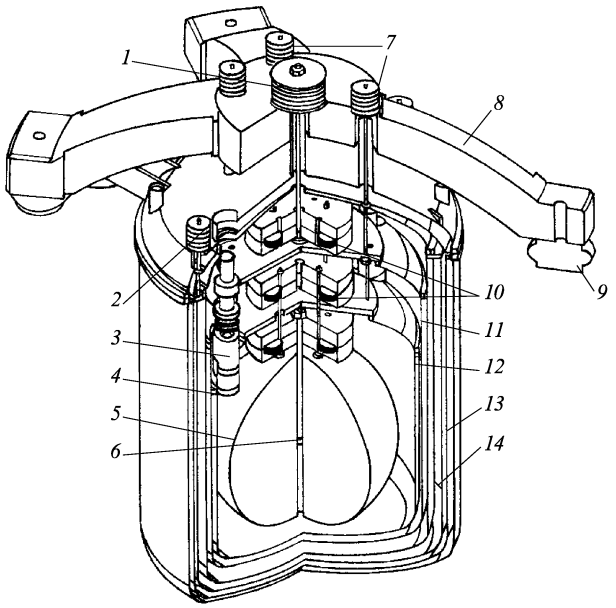

Figure 3. GRAIL: 100 ton 10 mK spherical antenna. *1*—rubber damper for sphere, *2*—rubber damper for helium vessel, *3*—dilution refrigerator anchored to shields, *4*—mixing chamber of DR (copper connections to shields and suspensions not shown), *5*—3 m diameter sphere (transducers not shown), *6*—copper rod suspension and thermal link, *7*—rubber dampers for copper shields, *8*—concrete support, *9*—air dampers, *10*—liquid-helium-filled bellows suspension, *11*—0.7 K copper shield, *12*—50 mK copper shield (Nb-plated for e.m. shielding), *13*—70 K shield, *14*—15 000 litre helium vessel (copper-clad stainless steel).

particularly CuBe and CuAl which are not superconducting and are about 3 times denser than Al 5056. Both Be and Al can dissolve in copper up to 10% giving sound velocities around 4700 m s^{-1} for CuAl, for Cu – 5% Be $v = 4300$ m s^{-1} and for Cu – 10% Be $v = 5300$ m s^{-1}. BeCu of lower concentrations was measured to have $Q \simeq 10^7$ [26].

At a density of 7.58 g cm^{-3} a CuAl sphere of 3 m diameter would weigh 107 tons. Fig. 3 shows a concept of such a detector called GRAIL (Gravitational Radiation Antenna In Leiden). A similar project will be developed for the successor of NAUTILUS. Other spherical detectors are under study in Louisiana, Stanford, Maryland, and Brazil.†

Let us discuss some of the important aspects of the GRAIL project.

(a) Cooling from room temperature to 4 K

The time constant for cooling a sphere from room temperature is given by $\tau = R^2/D$ where D is thermal diffusivity, $D = k/\rho c$, which for the alloy Al 5056 is $D = 4.5 \times 10^{-5}$ m^2 s^{-1} and for Cu – 10% Al is 1.76×10^{-5} m^2 s^{-1}. For $R = 1.5$ we have $\tau \cong 13$ h for Al 5056 and $\tau \cong 33$ h for CuAl. These values drop quickly with temperature, being a few seconds at 2 K. If we were to use the method of exchange gas as used with NAUTILUS, we see, by assimilating the bar to a sphere of radius 0.3 m that it would take about two years!

We thus have to cool the sphere by direct contact with cold helium gas, in a way similar to that used at CERN [27]. Cold helium gas should be circulated through a heat exchanger cooled by liquid N_2 and injected at high speed at the bottom of the sphere until $T \cong 80$ K is reached. At this point cooling should proceed from a 100 litre h^{-1} helium liquefier and it would require about 10 days to cool to 4 K. After pumping out the inner vacuum can (IVC) the sphere can be cooled in the usual way by contact with the DR. Cooling from 300 K to 4 K should last about 3 weeks. During pumpdown of the IVC the 15 000 litre helium vessel should be filled, and the liquefier disconnected from the cryostat to reduce vibrations.

(b) Cooling to 10 mK

The NAUTILUS experiment has shown that the heat leak to the bar is about 10 μW or 1.7 μW m^{-2}. For the sphere this would be 48 μW (supposing the heat leak is proportional to the area). Taking a factor of two for safety we require a cooling power of 100 μW at 10 mK, which is only a factor of four more than the refrigerators we have built at Leiden [19].

The circulation rate needed can be obtained from the expression

$$\dot{n} = \frac{\dot{Q}}{82T^2} = 3 \times 10^{-2} \text{ mol s}^{-1} .$$

This circulation will give a cooling power of about 100 mW at 200 mK.

For cooling from 1 K to 200 mK, one must remove

$$H = \int_0^T c_{\text{Cu}} \, \mathrm{d}T ,$$

with $c_{\text{Cu}} \simeq 10^{-4}$ J g^{-1} or $H \cong 10^4$ J. If we suppose the DR to be at 200 mK we need about one day to reach this temperature.

Cooling to 10 mK requires further removal of

$$H \cong \int_{0.01\text{ K}}^{0.2\text{ K}} 10^{-4} T \, \mathrm{d}T = 2 \times 10^{-6} \text{ J g}^{-1} ,$$

or 200 J, supposing the heat capacity is that of Al 5056 (we have no experimental data on CuAl at very low temperatures).

In this case, with enthalpy and cooling power decreasing as T^2 we need about one day to cool to ~10 mK. It thus seems that cooling the spherical 100 ton antenna to 10 mK can be done in less than one month. Great care must be taken in avoiding magnetic impurities which could increase the cooling down time at the low end by one or two orders of magnitude.

In the process of cooling with circulating helium gas it is important to avoid condensation impurities on the sphere and transducers, which could decrease the Q-factor. The use of a non-superconducting alloy with a thermal conductivity 100 to 1000 times higher than the Al 5056 alloy should provide a small (a few mK) thermal gradient across the sphere.

(c) Suspension

In order to measure a displacement of 10^{-22} m enormous precautions have to be taken to avoid external vibrations at the resonance frequency from reaching the antenna. If we assume a typical amplitude of 10^{-6} m at 1 KHz on the ground, we must have an attenuation of better than −320 dB or a factor of 10^{-16}. 160 dB can be provided by room temperature attenuators with rubber and steel stacks. An important precaution at room temperature is to decouple the boiling helium vessel from the sphere, as is shown in Fig. 3.

†We acknowledge helpful discussions with O D de Aguiar of INPE, Brazil, who is studying a similar detector.

The heat shields provide attenuation for the DR and are separately attached to the concrete structure. For larger attenuations the thermal noise becomes the dominant factor and damping at low temperature must be provided.

One interesting possibility is to use a new type of low-temperature vibration attenuator based on bellows filled with liquid helium.

At a pressure of 20 bar helium deforms by 15% as compared to steel with Young's modulus $E = 2 \times 10^{11}$ Pa which deforms by about 0.2% under maximum load.

If we take care to keep the pressure below solidification (say 20 bar) then the frequency of such a spring would be nearly 10 times less than that of an equivalent steel spring. The estimated attenuation per element of suspension (two copper plates containing eight 30 cm bellows) would be about 55 dB against about 30 dB for a similar but conventional suspension.† In this way one could hope for a total attenuation of say 160 dB at room temperature plus 165 dB due to the helium suspension and at least 70 dB due to the copper rod which holds the sphere. This is nearly 400 dB, at least on paper.

These suspensions offer the possibility of some external action. If some spurious resonance is close to the sphere resonance, changing the helium pressure could move it to a less dangerous place. Another possibility is to use a mixture of ^{3}He in ^{4}He which would allow the helium suspensions to act as nonmetallic thermal links between the copper plates and the DR. All we need is to use sintered silver inside the faces of the bellows support.

Conclusion

Cooling masses of 100 tons to millikelvin temperatures seems feasible and it represents certainly the largest-scale application of dilution refrigerators. These spherical detectors should open a new window on our Universe, creating an astronomy as important as radio or optical astronomy.

Acknowledgements

This preliminary study is being supported by the Dutch FOM foundation of NWO, by the National Institute of Nuclear and High Energy Physics of the Netherlands (NIKHEF) and by the University of Leiden. We gratefully acknowledge the INFN (Roma) for their continuous support of gravitation research in Italy and for their interest in this new antenna. The industry LIPS has done simulations of melting and solidification of large spherical CuAl objects as well as 50 cm diameter test model which shows the feasibility of the 100 ton cast. We are very happy to acknowledge their (free) help. A Marchenkov, A Simmons, V Stepankin, V Fafone, and J Noordhoek have contributed considerably to this phase of the GRAIL project and we thank them.

References

1. Blair D G (Ed.) *The Detection of Gravitational Waves* (Cambridge: Cambridge University Press, 1991)
2. Amaldi E, Pizzella G "La ricerca delle onde gravitazionali", in *Centenario di Einstein, Astrofisica e Cosmologia, Gravitazione, Quanti e Relativita* (Firenze: Giunti Barbera, 1979); Ruffini R "Sulla Astrofisica di oggetti stellari provenienti da fenomeni di colasso gravitazionale", in *Centenario di Einstein, Astrofisica e Cosmologia, Gravitazione, Quanti e Relativita* (Firenze: Giunti Barbera, 1979)
3. Misner C W, Thorne K S, Wheeler J A *Gravitation* (San Francisco: W H Freeman, 1973)
4. Weber J *Phys. Rev.* **117** 306 (1960)
5. Carelli P, et al. *Cryogenics* **15** 406 (1978); Suzuki T, Tsubono T, Hirakawa H *Phys. Rev. Lett. A* **67** 2 (1978)
6. Coccia E, Niinikoski T O *Lett. Nuovo Cimento* **41** 242 (1984)
7. Amaldi E, et al. *Astron. Astrophys.* **216** 325 (1989)
8. Amaldi E, et al. *Europhys. Lett.* **12** 5 (1990)
9. Hamilton W O, in *Near Zero, New Frontiers of Physics* (Eds J D Fairbanks, D S Deaver Jr, C W F Everitt, P F Michelson) (New York: W H Freeman, 1988)
10. Astone P et al. *Europhys. Lett.* **16** 231 (1991)
11. Braginsky V B, Khalili F Ha *Quantum Measurement* (Ed. K S Thorne) (Cambridge: Cambridge University Press, 1992)
12. Forward R *Gen. Rel. Grav.* **2** 149 (1971)
13. Wagoner R V, Paik H J "Experimental Gravitation", in *International Symposium Held in Pavia* (Acc. Naz. dei Lincei, 1977)
14. Brans C, Dicke R H *Phys. Rev.* **124** 925 (1961)
15. Coccia E *Rev. Sci. Instr.* **55** 1980 (1984)
16. Johnson W W, Merkowitz S M *Phys. Rev. Lett.* **70** 2367 (1993)
17. Weber J "Experimental Gravitation", in *International Symposium Held in Pavia* (Acc. Naz. dei Lincei, 1977)
18. Lounasmaa O V *Experimental Principles and Methods below 1 K* (London: Academic Press, 1974)
19. Vermeulen G A, Frossati G *Cryogenics* **27** 139 (1987)
20. Berglund P, Kyynäräinen J, Niinikoski T O, Rieubland J M, in *International Cryogenic Engineering Conference-9* (Guildford: Butterworths, 1982); Niinikoski T O, in *International Cryogenic Engineering Conference-10* (Guilford: Butterworths, 1984) and references therein
21. Coccia E, Niinikoski T O *J. Phys. E: Sci. Instr.* **16** 1983 (1983)
22. Bassan M, et al., in *5th Marcel Grossmann Meeting on General Relativity, Perth, Western Australia 1988* (Eds D G Blair, M J Buckingham, R Ruffini) (Singapore: World Scientific, 1989)
23. Coccia E, Modena I *Cryogenics* **31** 712 (1991)
24. Coccia E, et al. *Rev. Sci. Instr.* **63** 5432 (1992)
25. Coccia E, Pomentale T *CERN Internal Report (1982)* DD/82/16
26. Duffy Jr, W Preprint
27. Lebrun P, in *International Cryogenic Engineering Conference-15*

†We are grateful to A Semenov of the Kapitza Institute for Physical Problems, Moscow, for suggesting this possibility.

PACS numbers: 07.55.Db

Recent progress in high field magnetism

M Date

Abstract. This paper describes recent progress in high field magnetism mainly done in the Research Centre for Extreme Materials, Osaka University, with a short survey of the history. The main activities are concentrated on the condensed matter physics covering the field of magnetism and superconductivity where a common keyword is 'highly correlated electron physics'. A wide range of studies of metamagnetism, field-induced electronic transitions under high field, is summarised. These high field states are regarded as field-induced quantum states with various

novel properties. High field is also effective for various atomic and molecular sciences. Nonlinear Zeeman effect, field-induced transparency and diamagnetic orientation of organic and biological materials are shown as examples. New frontiers in the high field technologies are shown with a highly sensitive magnetometer using the dynamical Faraday effect.

1. History of high magnetic field generation

There has been growing interest in the application of high magnetic fields to the study of magnetic properties of various materials mainly because the field can produce intrinsic change not only in the magnetic structures but also in the electronic states of highly correlated electrons.

Nowadays, one can produce DC fields of more than 30 Tesla (T), pulsed fields of more than 70 T and about 500 T can be reached with magnets that are destroyed in the process.

The history of generating high magnetic fields began with the discovery of Oersted in 1820 who found the first 'artificial' field by passing an electric current. The second step was to concentrate the magnetic flux by using ferromagnetic materials as was done by Faraday and others. The method was improved by Ewing around 1890 who attained a maximum field of 3.5 T and discovered the ferromarnetic saturation phenomenon [1]. A conventional electromagnet at the end of the 19th century could provide a field up to 1 T.

Innovative progress was achieved by Kapitza who produced a pulsed magnetic field up to 35 T by transforming mechanical energy of a motor generator into magnetic energy in 1924 [2]. The DC-field, on the other hand, was improved by Bitter around 1940 with a water-cooled Bitter coil which could produce about 20 T [3]. A similar field is now produced by superconducting magnets and they are used world-wide since 1960. The maximum DC-field has been obtained with a hybrid magnet consisting of the Bitter and superconducting magnets with net fields of the order of 30 T.

During the Second World War, a new idea of generating strong magnetic fields by compressing magnetic flux by the implosion technique with the use of gunpowder was advanced [4]. A similar compression method was invented by Cnare, who used the electromagnetic force. The method is being developed at ISSP by the Miura Group [5]. These methods can produce about 500 T for several microseconds with destruction of the coil system and so are for precise measurements.

In 1970, the present author proved a theorem that an infinite magnetic field can be produced nondestructively when a specially designed multilayer coil is used [6]. The practical design and construction of the new coil were implemented and a series of nondestructing multilayer coil magnets was produced at Osaka University. The magnets have been used by many researchers and more than 300 papers in the fields of condensed matter physics, chemistry, and biology have been reported since 1975. A short review of the magnets is presented in the next section and the details are given in two papers [7, 8].

2. Osaka magnet — multi-layer coil system

It is impossible to produce an infinitely strong magnetic field in a coil without destroying the system because of the strong electromagnetic force acting on the magnet. Kapitza was aware of the difficulty, with the conclusion that the highest field to be practically possible to produce may be around 50 T even if the strongest material, for example steel, were used. We call this the Kapitza limit. As is shown in Fig. 1a, the force is axially compressive while it is expansive along the radial direction. The force is about 400 kg mm^{-2} at 100 T, which is about four times larger than the tensile strength of normal steel.

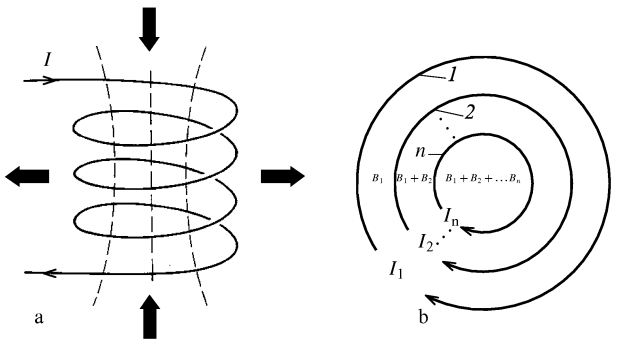

Figure 1. (a) Force acting on a coil and (b) schematic model of the multi-layer magnet.

In 1970 – 1975, the present author developed a set of multilayer coil systems based on the theorem that one can produce an infinitely strong magnetic field without destroying coils if a specially constructed multilayer coil is used. The central idea is illustrated in Fig. 1b where each circle represents an independent magnet coil. Coil *1* produces the field B_1 by a current I_1. B_1 may be around 50 T, within the Kapitza limit. The second coil *2* inside coil *1* produces the field B_2, but B_2 should be smaller than B_1 because the electromagnetic force acting in coil *2* is proportional to $B_1 + B_2$. Numerical calculation shows that $B_2 = 0.62\,B_1$ for

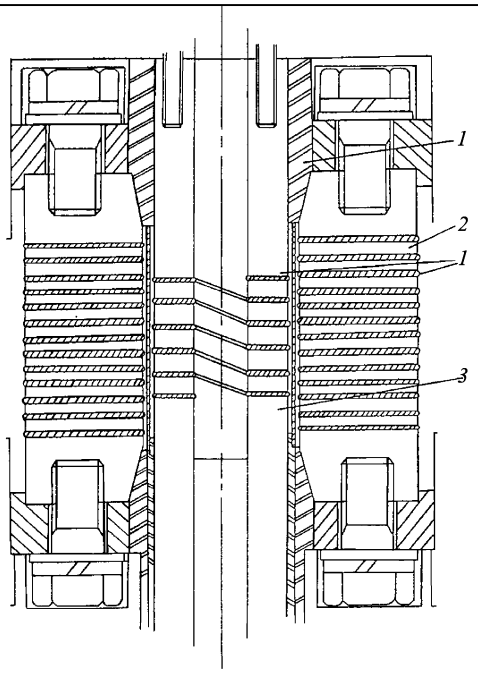

Figure 2. Section view of the standard 2-layer magnet: *1* — insulator, *2* — outer coil, *3* — inner coil.

the safety limit of coil 2. Coils 3 ... n are designed in a similar fashion and the expected resultant field B_r in coil n obeys the relation:

$$B_r > B_1\left(1+\frac{1}{2}+\ldots+\frac{1}{n}\right). \quad (1)$$

This means that B_r tends to infinity as $n \to \infty$. We have constructed various multilayer magnets based on this theorem and a test magnet with $n=4$ produced a maximum field of 107 T in a volume 2 mm in diameter [6]. The practical magnet now widely used is a two-layer one 2 cm in inner diameter, and a section view is shown in Fig. 2. The maximum field is 70 T with a pulse direction of about 1 milli-second [7]. An advanced three-layer magnet has recently been constructed which can produce more than 80 T.

International use of the Osaka magnet has been made since 1975 and more than a thousand scientists have visited the facility. The main results obtained by them have been reported in several papers [8–17] and the recent highlights are shown in the following sections.

3. Classical problem — spin rearrangement in high field

Around ten years ago, the main scientific results obtained in the early stage of the high magnetic field facility were limited to the field-induced magnetic phase transition, i.e., spin rearrangement such as the antiferromagnetic spin-flip. Two typical examples are shown in Figs 3 and 4. The dM/dB signals shown in Fig. 3 were obtained in the antiferromagnetic MnF_2-FeF_2 system when the field was applied along the spin easy axis. The work was done with the cooperation of the Jaccarino group in Santa Barbara [18]. The sharp spike at $x=0$ refers to spin-flip in MnF_2 at 8 T. The peak becomes broad in the mixed crystals owing to the random field effect and again becomes sharp at $x=1$ for FeF_2 at 42 T. The magnetisation profile of the triangular antiferromagnet is shown in Fig. 4 for the example of EuC_6, a graphite intercalation material [19]. The data were obtained in cooperation with the Suematus group of Tsukuba University. Various extensive studies on the magnetic phase transition in this area have been done in Osaka on ferromagnetic, metamagnetic, and helical magnet materials. These problem are now called classical because the transitions are described by the spin rearrangement alone.

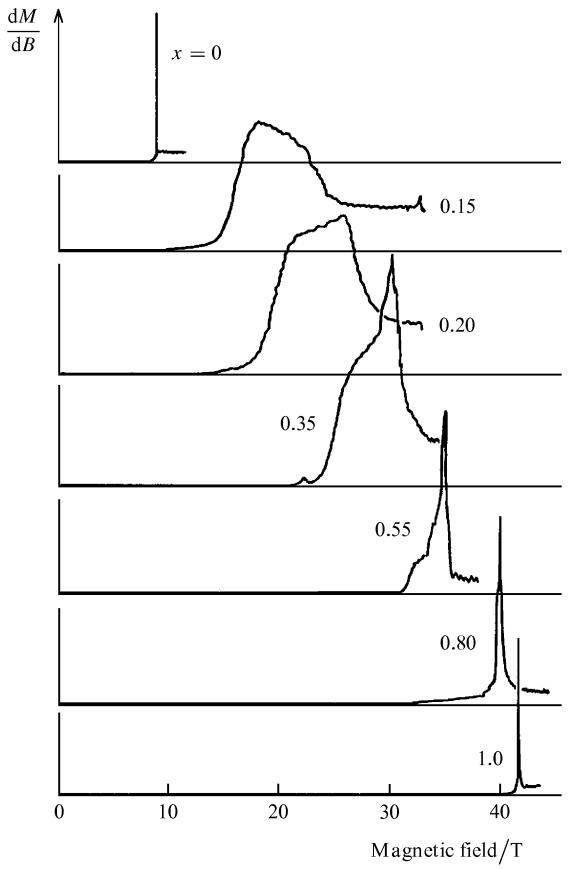

Figure 3. Differential magnetisations in $Mn_xFe_{1-x}F_2$; $T=4.2$ K.

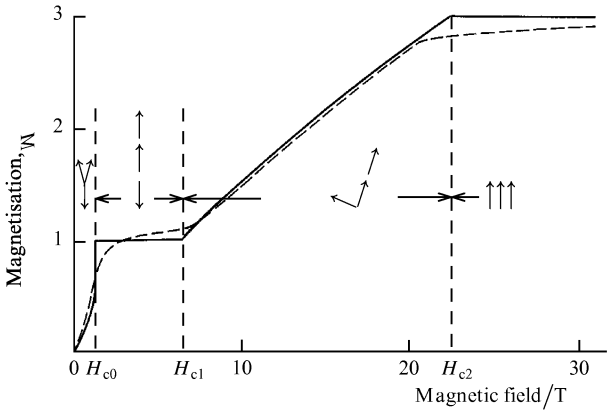

Figure 4. Magnetisation process of a triangular spin system, EuC_6.

4. Modern problem — field-induced electronic state

A noticeable trend in recent high-field magnetism is the attainment of a new quantum electronic state induced by applying a high magnetic field. The subject has become popular as the maximum attainable field intensity increased. Typical examples in this category are given in this section.

(1) Crossover of the atomic ground state

A magnetic field can induce ground state crossover in some atoms and molecules. An example is given where the angular momentum change from $J=1$ to $J=2$ occurs on applying a field. $CsFeCl_3$ is a hexagonal antiferromagnet with Fe^{2+} spins where the ferromagnetic chains along the c-axis are connected by a triangular antiferromagnetic interaction. However, no long-range order is found at low temperatures because of the singlet ground state with $J_z=0$, which is a sublevel of $J=1$. Under a magnetic field, the first crossover occurs around 10 T in the framework of $J=1$ [20] with the net moment of about $3\mu_B$. A new multistep magnetisation is found above 32 T along the c-axis and it is explained by the crossover from $J=1$ to a sublevel of $J=2$ [21]. The central idea of the transition is simply explained in Fig. 5. The angular coupling of L and S in the $J=2$ state given in Fig. 5a shows the presence of a transverse component of the spin which is not found in the $J=1$ and $J=3$ states. The exchange energy proportional to the transverse component should be taken into account for the c-plane. The analysis was done by the present author [21] and the result is shown in Fig. 5b. Multistep magnetisation with the moments 1/3,

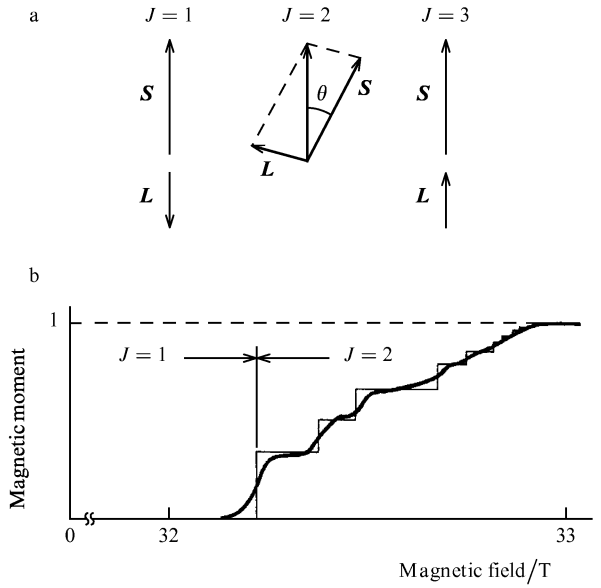

Figure 5. (a) Vector model of the Fe spin in $CsFeCl_3$ and (b) the multistep magnetisation due to $J = 1 \rightarrow J = 2$ crossover.

1/2, 2/3, ..., is found as expected from the theory and the agreement between theory (thin line) and experiment (thick line) is surprisingly excellent as is seen in Fig. 5b. The various fractional states appear by the spin frustration in the mixed states of the ground ($J = 1$) and excited ($J = 2$) spin chains.

(2) Quenching of the Haldane state under high field

There has been an increasing interest in the energy gap in the linear-chain Heisenberg antiferromagnet with spin $S = 1$ since Haldane conjectured that the chain consisting of integer spins has an energy gap above the ground state. A high field magnetisation study up to 50 T has been done by Katsumata et al. [22] as is shown in Fig. 6 and the field-induced quenching of the gap is found in NENP, one of the best materials to show the Haldane state. The quenching is characterised by the critical field above which the system is in the usual antiferromagnetic state. Electron spin resonance of this material under high field was studied by our group [23] and the anisotropy parameters of the first excited state were investigated. A striking fact is that the sign of the anisotropy constant D in the ground state of Ni^{2+} is positive while that of the excited state triplet is negative. The result is explained by introducing a model in which the excited state is at two-spin bound state with the resultant spin $S = 1$ moving in the chain like a soliton [23]. The ESR data were analysed by use of the theory of spin-cluster resonance [24] with a satisfactory agreement.

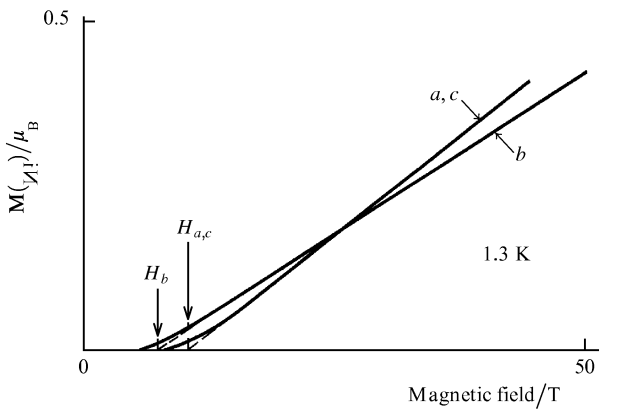

Figure 6. Quenching of the nonmagnetic Haldane state in NENP. Linear magnetisation appears above the critical fields H_a, H_b, H_c showing normal antiferromagnetism.

(3) Quenching of the quadrupole order in DyAg

A multistep magnetisation observed in DyAg presents a new concept for high field magnetism. An example of the data is shown in Fig. 7 where stepwise magnetisation with the magnitudes 1/2, 2/3, 5/6, and 1 are illustrated. The thick line shows the experimental result and the theoretical steps given by thin lines are given by the following model. DyAg is a CsCl-type crystal with an antiferromagnetic transition at $T_N = 55$ K. Spins are parallel to four $\langle 111 \rangle$ directions with the four-sublattice model [25]. A large quadrupole energy stabilises the spin structure. The observed step magnetisation is explained by keeping the quadrupole energy on each Dy site but we assume that there is a quadrupole coupling energy between neighbouring Dy spins with the form of $(3\cos^2\theta_{ij} - 1)\,Q_{ij}/2$, where Q_{ij} is the quadrupole coupling constant between i- and j-spins and θ_{ij} is the angle between spins. The total energy is calculated as the sum of the exchange, quadrupole, and Zeeman energies and the standard mean field model is applied. The experimentally obtained steps are explained by a simple spin-flip at the $0 \rightarrow 1/2$ transition and the successive three transitions are given by the spin-flip with the rearrangement of the quadrupole order. Agreement between theory and experiment is satisfactory as is seen in Fig. 7. Three exchange parameters and three quadrupole coupling constants have been determined by this treatment [26]. Thus, DyAg provides a typical example of the quenching of the quadrupole order under a high magnetic field.

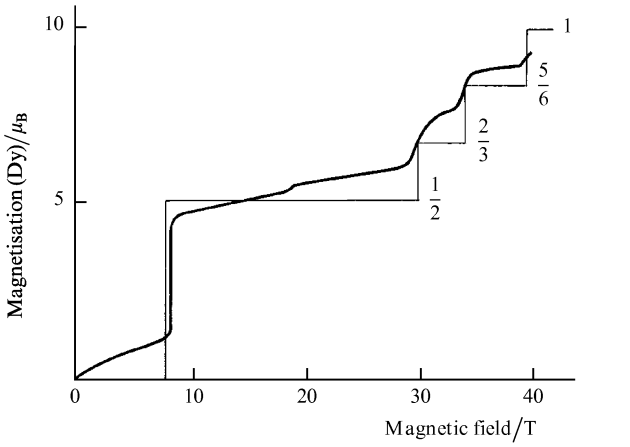

Figure 7. Multistep magnetization of DyAg along the [111] axis, $T = 4.2$ K

(4) Multistep magnetisations in CeP

Recently, a high quality was achieved in single crystals of CeP with RRR 50 and the Shubnikov–de Haas (SdH) oscillations. An unusual metamagnetism has been observed, as shown in Fig. 8 [27]. The metamagnetic transition fields are almost temperature independent from 1.3 to 35 K and

lie with equal spacing on the H^{-1} scale. This result is explained in terms of the Stoner–Landau model. Namely, the magnetic transition of localised Ce spin is related to the Landau-level crossing of up and down spin bands which one separated by the Stoner gap. The angular dependence of the multisteps were also investigated and a simple cubic symmetry with fourth-order anisotropy was found. The multisteps found in CeP provide the first example of the successive phase transition induced by the de Haas–van Alphen change in the conduction electrons.

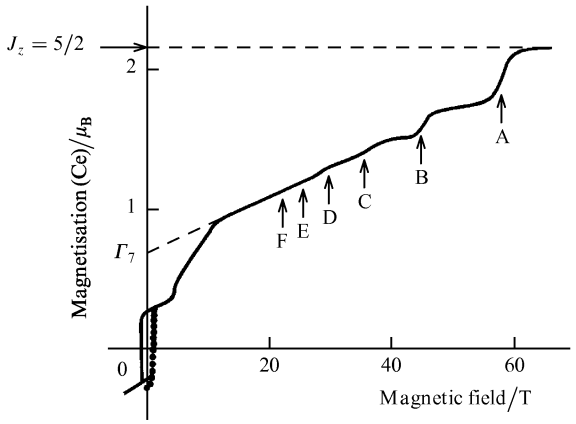

Figure 8. Multistep magnetisation of CeP. Peaks A, B, ..., F are Ce-spin steps induced by the de Haas–van Alphen oscillations of conduc-tion electrons.

5. Physics in highly correlated electron systems

One of the recent directions in condensed matter physics is the study of highly correlated electron systems where the heavy fermions or high-T_c superconducting electrons play an important role. A high magnetic field is effective for these electrons because the field destroys their coupling and the elementary processes or couplings are separated by applying the field. A schematic picture is given in Fig. 9 where the gap structure or dense Fermi-level states produced by their correlation are destroyed by applying the field.

Two examples of heavy fermion materials are discussed below.

Much work has been done on the study of heavy fermion materials in high magnetic fields and the metamagnetic nature has been observed in some compounds. URu_2Si_2 is known as a typical material with a clear three-step metamagnetism around 30 T [28]. A detailed study has been done by our group and the observed data are well explained by the model in which the heavy fermion state in the low field region is destroyed by applying a strong magnetic field, and the exchange interactions between the field-induced magnetic moments on the uranium atoms produce successive metamagnetic transitions [29]. The localised magnetic moment on the uranium atom at zero magnetic field is only $0.03\mu_B$, reflecting the fact that the f-electrons are not on the uranium site but form a heavy fermion band with conduction electrons. Under a strong magnetic field, however, the Zeeman energy of the f-electron exceeds the heavy electron coupling energy and a phase transition to the magnetic state occurs. It is noted that there is a frustrating exchange coupling between the field-induced moments and the metamagnetic three-step states with the moments 1/3, 3/5, and 1 (ferromagnetic) that appear at their corresponding critical fields. The observed data (thick line) and the theoretical three steps are shown in Fig. 10a. The heavy fermion energy and three exchange coupling parameters are determined by the standard mean field approximation. It is emphasised that the present treatment is applicable when the spin system can be regarded as an Ising network, where a sharp transition is expected.

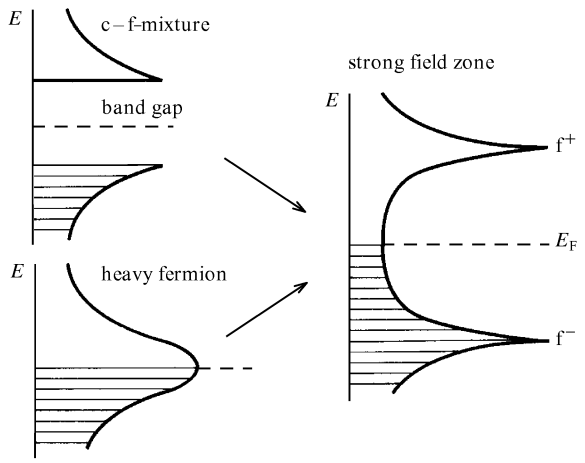

Figure 9. The c–f mixed density of states (left) are modified by applying high field (right) where the f-bands are separated from a normal conduction electron band.

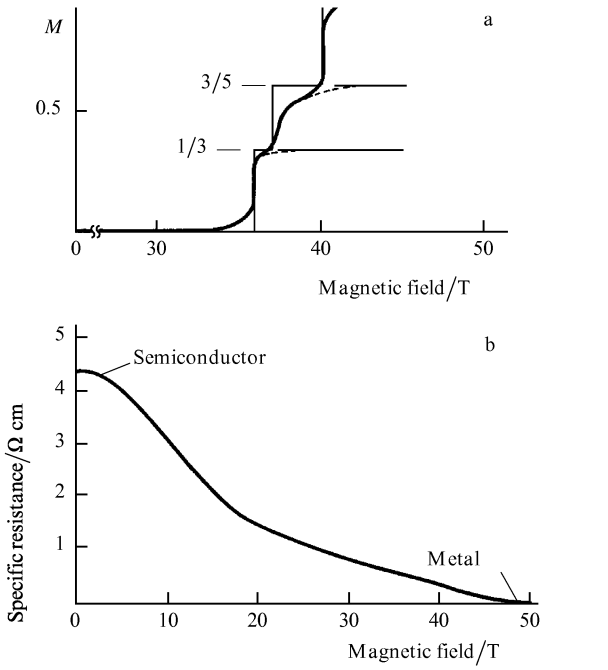

Figure 10. (a) Three-step magnetisation in URu_2Si_2. Thin lines show the theoretical expectation. (b) The negative magnetoresistance in YbB_{12}, which is perfectly metallic above 50 T.

Quenching of the electronic band gap by a magnetic field is usually difficult even when fields up to 100 T are used. An exceptional success was achieved with YbB_{12}, which has a gap of about 100 K above the Fermi level. The origin of the gap is believed to come from the hybridisation of the f- and conduction bands. The electric resistivity was measured in fields up to 50 T and a large negative magnetoresistance was found as shown in Fig. 10b. The resistivity is immeasurably small and the compound is substantially metallic around 50 T [30]. The observed result is well explained by the quenching of the hybridised band due to the magnetic field. The Zeeman energy of the f-electrons plays an important role in this phenomenon. This model is supported by the high field magnetisation experiment where a clear increase in the magnetic moment appears above 50 T. A similar effect is expected for SmB_6, a typical semiconductor with a band gap due to the hybridisation, but the observed magnetoresistance a tenth of that in YbB_{12}. The difference is due to the magnitude of g-values in the two materials.

The next example is the high field effect in high-T_c superconductors. Much work on the determination of the upper critical field H_{c2} of the oxide high-T_c superconductors has been reported since their first discovery in 1986. In these experiments, however, the whole profile of the magnetoresistance curves has been obtained only by our group [31] because H_{c2} of these materials at low temperatures is much higher than the limit for the usual superconducting magnets. It is emphasised that the whole aspect of the magnetoresistance in all 123-compounds can be obtained even at 4.2 K when a field up to 60 T is applied. The studied high-quality single crystals were grown by the NTT research group [32]. Their thickness was about 0.02 mm, small enough to avoid eddy current effects and hysteresis.

As the magnetic field becomes strong enough to break up the superconducting state, one can determine the temperature dependence of the normal electric resistivity for these compounds and the results are given in Fig. 11b [33]. The full lines are the results of the usual measurement and the dashed lines below T_c are obtained by extrapolating the high-field magnetoresistance curves to the zero-field value. The whole behaviour of the resistivity shows that the 123-compounds are rather similar to normal metals which display constant resistivity due to impurities at low temperature.

Recently, a single crystal of the high-T_c superconductor $Nd_{2-x}Ce_xCuO_y$ has been studied in high fields up to 20 T. The superconducting state completely collapsed and the normal electric resistivity persisted at all temperatures as shown by the dashed line in Fig. 11a. The temperature dependence of the normal resistivity down to 1.3 K shows a clear minimum. The result can be understood in terms of the two-dimensional weak localisation model [34], which means that this material can be regarded as an intrinsic two-dimensional conduction system.

The resistivity minimum is not observed in 123-compounds where the residual resistivity is small and constant. According to the weak localisation theory, the resistivity increase at low temperature does not occur when the residual resistivity is small. This fact explains well the results and the two-dimensionality of 123-compounds is not contradicted.

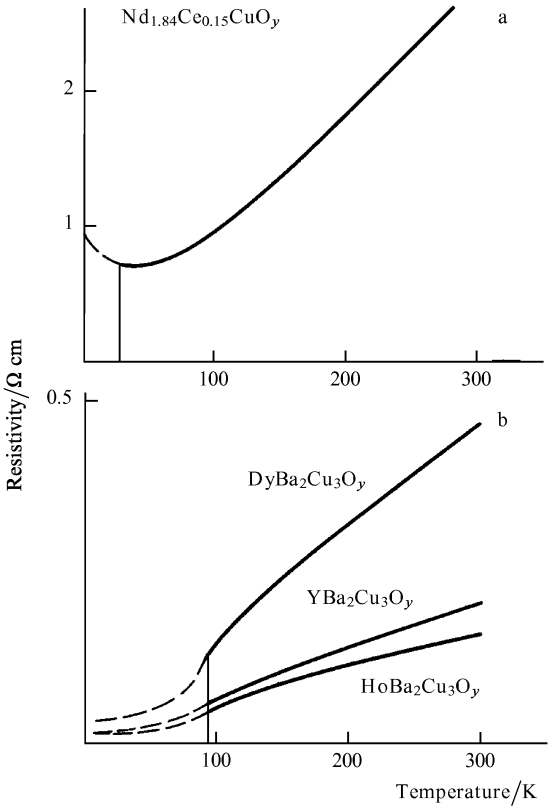

Figure 11. (a) Temperature dependence of the resistivity in an oxide superconductor. The dashed line is observed under high fields (perpendicular to the *ab* plane). (b) The electric resistivity of three 123-compounds. The dashed lines are obtained around 50 T.

6. Field-induced crystallographic transformations

It is generally difficult to induce crystallographic transformations by applying a magnetic field. An exceptional case is the field-induced martensitic transformation. Systematic studies of various alloys have been carried out by the Shimizu group in Osaka. A striking effect was found in Fe–Ni alloys where the martensitic transformation temperature increased by more than 80 K in a field of 40 T [35].

Another interesting change in the crystallographic modification was observed in $DyCu_2$ [36]. $DyCu_2$ is an intermetallic rare-earth compound with the orthorhombic $CeCu_2$-type crystal structure. The Neel temperature is 31.5 K and the Dy spin has an Ising-like axis along the *a*-direction with two-step metamagnetism at low fields, as shown in Fig. 12. The gJ-value along the *a*-axis is about 10 in accord with the usual Ising-like Dy^{3+} spin. Magnetisations along the *b*- and *c*-axes are smooth and weak in low fields, as shown in Fig. 12.

In high magnetic fields, however, this material shows a peculiar behaviour given in the right plot of Fig. 12. The *c*-axis magnetisation is as expected up to 13 T but a sudden jump in the magnetisation occurs around 13 T to the level of the saturation moment along the *a*-axis. The magnetisation curve under a decreasing field is different from that along the *c*-axis but is very close to the *a*-axis magnetisation, which is called *a*-like (a') in Fig. 12. After this procedure, a low field magnetisation up to 3 T leads to the switching of the *a*- and *c*-axes but the *b*-axis remains unchanged. The recovery to the virgin state is obtained

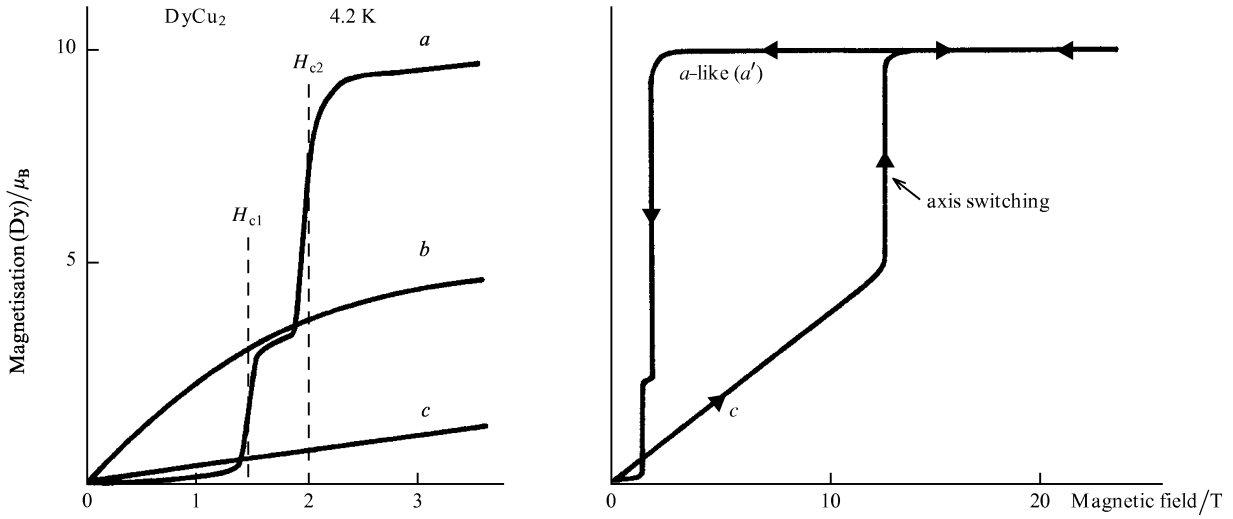

Figure 12. Metamagnetic transition and Ising axis switching in $DyCu_2$.

either by warming the crystal above about 100 K or applying a field higher than 5 T along the *a*-axis. The c'-axis, which is the original *a*-axis, shows a weak magnetisation up to 5 T, where a sharp step magnetisation appears, and then a decrease of the field clearly brings about a typical *a*-axis magnetisation reflecting return to the virgin state.

Note that the switching cycle can be observed by rotating the crystal in liquid helium because temperature increase also results in the recovery process.

The observed process, called switching of the magnetic axis, is explained by a first-order transition model similar to the model of the field-induced martensitic transition [36].

7. Atoms and molecules under high magnetic field

A high magnetic field can help us to understand a large range of properties of atoms and molecules. The standard technique is to observe linear and nonlinear Zeeman effects with the use of various electromagnetic waves and much work in this case has been reported.

A unique discovery has been the field-induced transparency in liquid oxygen done by our group [37]. The ground state is expressed as $3\Sigma_s$. The boiling point of liquid oxygen is 90 K, below which the liquid has a blue colour. Under a magnetic field, however, the blue colour is quenched and the liquid becomes transparent. The field-induced transparency is nicely explained in the following way: the blue colour comes from the two-molecule absorption of light with a zero net spin moment. Under high magnetic field, however, all spin moments are parallel so that the light absorption is forbidden and the liquid becomes transparent. This is the only example of field-induced colour change in condensed matter known at present, if one disregards the virtual colour change of liquid crystals due to reflection.

The second topic in this section is the diamagnetic orientation of organic molecules under a magnetic field. Except in the superconducting state, the diamagnetism of molecules is generally weak and no important physical and chemical effects have been reported. In high magnetic fields, however, the diamagnetic energy is not negligible and various new phenomena have been investigated recently. Let us consider two examples. One is the diamagnetic Curie–Weiss law found in an organic liquid and the other is the diamagnetic alignment of biological materials related to human blood. Consider a benzene molecule under a magnetic field. As the diamagnetic shielding current flows in the benzene ring, a field-induced diamagnetic moment appears in the molecule. Its magnitude is maximum when the field is perpendicular to the ring plane. Therefore, the field energy is maximum in this case and is minimum when the field is parallel to the plane. Accordingly, the ring is stable when the plane is parallel to the field. The magnitude of the anisotropy energy is, however, very small and only one molecule per 10^6 molecules aligns in this manner at room temperatures under a field of 100 T. The alignment effect can be detected by observing the Cotton–Mouton effect in the liquid. The effect is measured by looking at the rotation angle of the polarisation plane of the incident light under the field; this angle is proportional to the diamagnetic anisotropy χ_a of molecules. At the beginning of this century, Langevin pointed out that χ_a is inversely proportional to temperature T [38]. At that time, however, the attainable magnetic field was not so strong and the higher-order effect could not be detected. As the Cotton–Mouton effect is proportional to B^2, a high magnetic field is very effective and a series of precise measurements has been done in Osaka for many organic liquids [39]. The results show that χ_a is proportional to $1/(T-\Theta)$, which is formally similar to the paramagnetic Curie–Weiss law. So, we called this the diamagnetic Curie–Weiss law and the Curie–Weiss constant Θ has been measured for many liquids. A theoretical extension has been also done and it is now clear that Θ represents intermolecular interactions. Θ is almost zero for benzene but is 165 K for nitrobenzene. This means that intermolecular interaction in nitrobenzene is stronger than in benzene liquid. The interaction is ranked as a quadrupolar interaction in liquid.

When diamagnetic anisotropic molecules are connected and aligned with their anisotropy axes in a definite direction, the net anisotropy increases with increasing molecular number. There are some examples especially among biological materials. The first clear example was found in Grenoble, France, with fibrin, an organic macro-

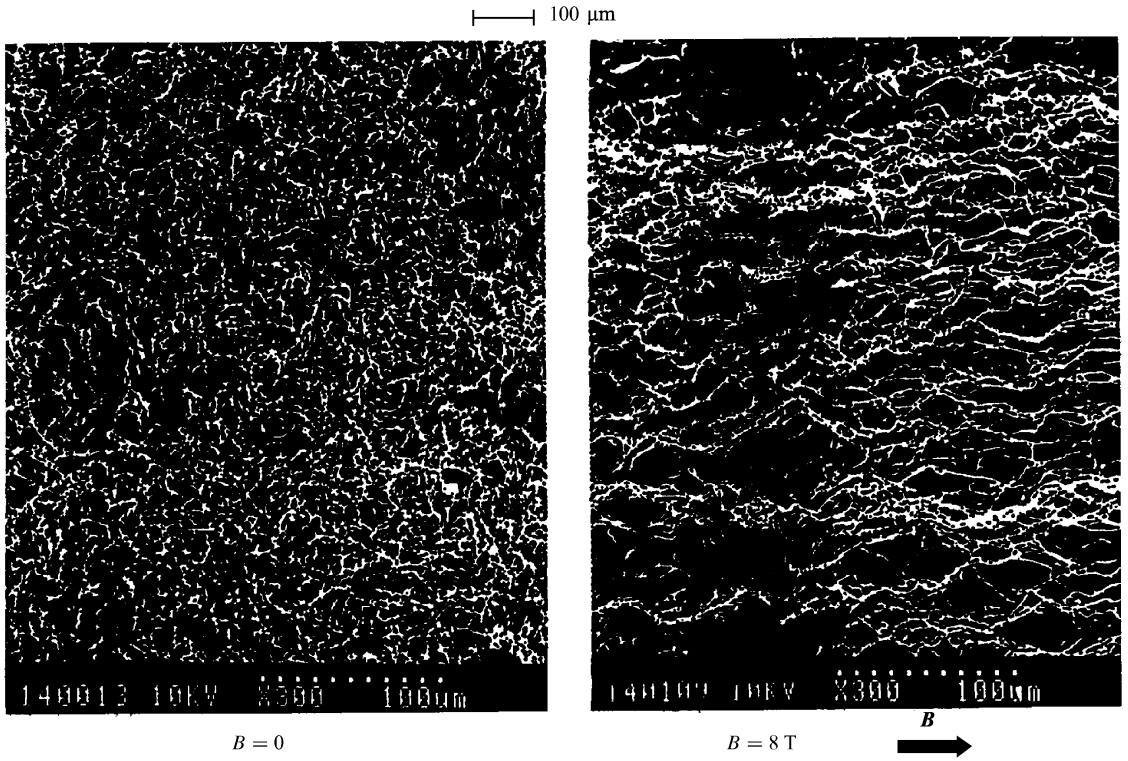

Figure 13. Diamagnetic orientation of fibrin fibres. The fibre orientation is random in zero magnetic field (left) while good alignment along the field is seen on the right.

molecule in human blood whose function is to coagulate blood in case of injury. A photograph taken in Osaka is shown in Fig. 13. The work has contunued in Osaka and a typical alignment effect has been found in human red blood cells. The diamagnetic alignment occurs from only 1–2 T and this means that a macromolecule consists of more than 10^7 unit molecules [40]. The details are not shown here, but the alignment suggests that the effect of a field on the human body might not be negligible even if the field is not very strong. The effect of magnetic field on the human body has attracted much attention not only by scientists but also by many others. However, no clear evidence has yet emerged. The diamagnetic alignment effect reported here can be regarded as a breakthrough in this problem. The effect of high fields on the human body—magnetobiology—can be further investigted on the basis of such a clear physical fact.

8. New technologies involving high magnetic fields

A high magnetic field is useful not only in basic science but also in advanced technologies. Various kinds of technological applications are in progress. We show here only one example. It is noticed that high field generation also produces high field gradient dB/dz, and this is useful for highly sensitive magnetometers. A paramagnetic or diamagnetic material feels a force proportional to $B\,dB/dz$. Historically speaking, Faraday constructed a magnetometer using this relation and it is now called the Faraday method. In a pulsed field, the value of $B\,dB/dz$ is about 10^4 larger than in the usual Faraday magnetometer. We have constructed a magnetometer, shown in Fig. 14, which uses a pulsed field and the method is called the dynamical Faraday method [41].

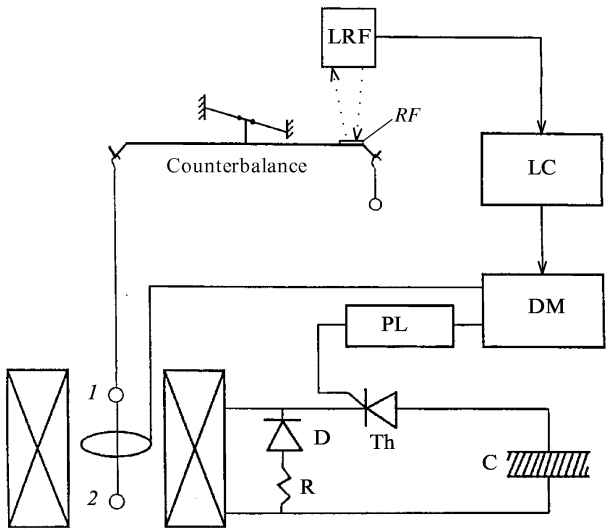

Figure 14. Block diagram of the dynamic Faraday method. A specimen is set at *1* and a counter-balance material is set at *2*. PM and the connecting materials are the pulse-magnet and the accessories.

After one shot of the pulse field, a paramagnetic or diamagnetic specimen on one arm of a balance acquires a momentum due to acceleration by $B\,dB/dz$ and begins to oscillate. An example is shown in Fig. 15 where a thin diamagnetic hair of 1.92 mg is set on the balance. The magnetic susceptibility of the specimen can be measured by observing the oscillation and the obtained sensitivity is about 10^3 times higher than that of a SQUID magnetometer. We are now measuring a slight change in biological materials after a light flash or physiological shock. This is only one

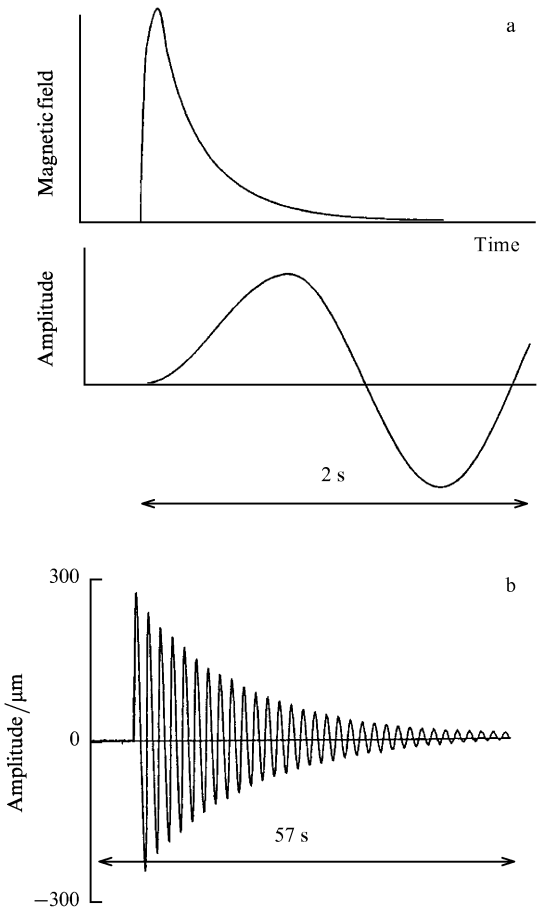

Figure 15. (a) Pulse field profile and oscillation of the balance. (b) The long-time oscillation profile.

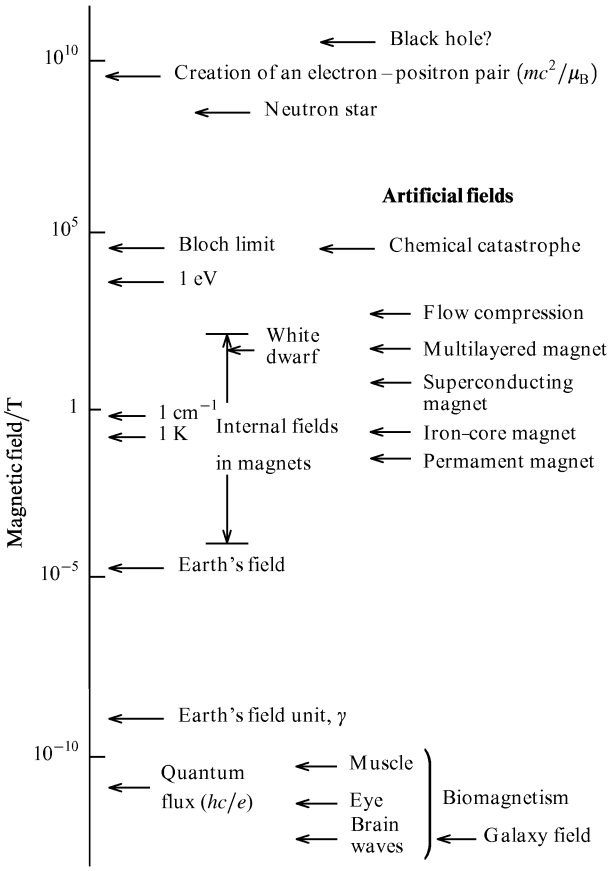

Figure 16. Natural and artificial magnetic fields.

example, and we expect wide possibilities for applying the highly sensitive pulse field magnetometers.

9. High fields in the future

We have outlined the frontiers in high magnetic field sciences and technologies. They are now progressing rapidly and expanding to new fields. It is difficult to forecast the future development but it may be valuable to survey the whole of high magnetic field science with a bird's-eye view. Fig. 16 shows various natural and artificial magnetic fields and the corresponding physical phenomena at all possible field strengths on a logarithmic scale. The energy units in terms of one electron spin Zeeman energy are given on the left. For example, it is convenient to remember that 1 T is comparable with 1 K and 1 cm^{-1}. A quantum magnetic flux (hc/e) through an area of 1 cm^2 corresponds to a field strength less than 10^{-10} T. This is the lowest flux density that can be determined practically and the corresponding detector is a SQUID. It can detect a field change of about $10^{-2} - 10^{-3}$ of quantum flux and various types of biomagnetism: electric currents induced by magnetic fields associated with brain waves, produced by eye movements or muscle actions, have been observed. These are the lowest fields that can be detected at present. By the way, the Earth's magnetic field unit γ (10^{-9} T), defined as a quantity of the order of Earth's field fluctuations, was the lowest detectable field before discovery of the quantum flux. There are various magnetic fields in magnetic materials. The highest field is the exchange interactions for example in ferromagnetic iron-cobalt alloy, and various magnetic anisotropy fields, dipolar fields, and hyperfine fields are included in this category. These fields are rich in variety and more are being investigated. Their study is also important for magnetic technologies.

Artificial fields are shown on the right. Permanent magnets and iron-core magnets lie in the Tesla region and superconducting magnet can produce fields stronger by one order of magnitude. Our multilayer magnet covers up to 100 T and flux compression can produce about 500 T, which is the maximum at present.

On the other hand, natural magnetic fields have a wide variety. The Earth's field is of the order of one gauss (10^{-4} T), which has been a standard magnetic unit. The solar field near a black spot is about 0.5 T, the largest field in the solar system. Outside the solar system, however, there are very strong magnetic fields in high-density stars, white dwarf having fields higher than 100 T. It is believed that these stars have high material density induced by the collapse of atoms due to high gravity and the strong field is produced by flux compression associated with the collapse. The next stage is the collapse of nuclei or, more exactly, melting of nuclei to a neutron sea where an electron is captured by a proton forming a neutron. This is a neutron star where the flux compression is believed to be huge, of the order of 10^9 T. The famous black hole is still above it. However, black holes are difficult to observe and nobody knows their magnetic field. These fields may or may not exist: it is still an open question today. It is noted that electron pair creation energy is close to this field strength. This means

that the Zeeman energy of an electron–positron pair with parallel spin is smaller than the annihilation energy with the formation of vacuum.

Human achievement measured by the level of magnetic field strength is thus very low at present. We must admire Mother Nature, her depth and capacity. However, we are optimistic about future human possibilities for the following reason. Progress in magnetic field generation technology in the past two centuries has been linear on the logarithmic scale: the maximum field at the end of the 18th century was 10^{-2} T and 1 T at the end of the 19th century. Now, in the 20th century, it is substantially around 100 T.

Therefore, optimistically speaking, it will be 10^4 T at the end of the 21st century. If this were achieved, high field science would enter a new world because this field is close to the boundary of the chemical catastrophe. What is meant by the chemical catastrophe? The boundary means that the spin Zeeman energy is comparable to the chemical binding energy. Therefore, all atoms and molecules become unstable because the spin-paired bound state will no longer be stable. We now have no information what materials and phases are possible under these conditions. Another interesting world will be revealed at the Bloch limit at which the first Landau level orbit has an area equal to that of the crystallographic unit cell. What happens here? Hofstadter predicted that the electronic band structure will be reduced in the field and he drew the band structure shown in Fig. 17 [42]. The field-induced band reduction is one of the interesting high field effects. It is predicted that there will also be a big change in atomic and molecular hydrogen. The shape of the hydrogen atom in the ground state is spherical but it will become prolate along the magnetic field. Furthermore, in a neutron star, the shape will be needle-like due to strong squeezing by the field. A hydrogen molecule in the chemical catastrophe region would be in the triplet ground state because the singlet is not stable.

Thus, the goal of the study of high magnetic fields is long term, spanning centuries.

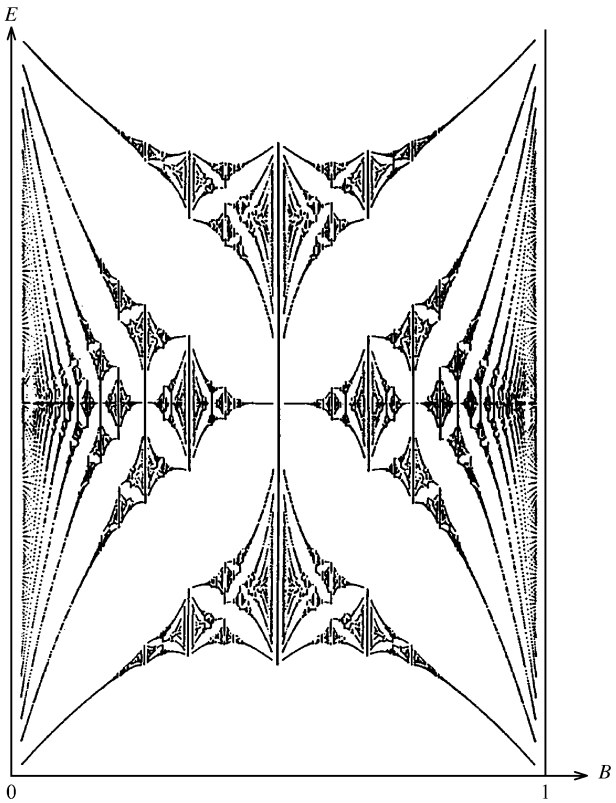

Figure 17. Band structure of a simple cubic metal under magnetic field B drawn by Hofstadter. B is normalised so as to be unity when the Landau orbit and a face of the unit cell have same area.

References

1. Starling S G *Electricity and Magnetism* (London: Longmans, 1925) p. 285
2. Kapitza P L *Proc. R. Soc. (London) Ser. A* **105** 691 (1924)
3. Biter F *Rev. Sci. Instr.* **10** 373 (1939)
4. Fowler C M, Garn W B, Caird R S *J. Appl. Phys.* **31** 588 (1960)
5. Miura N, Gotto T, Nojiri H in *Proceedings of the 6th International Conference on Megagauss Fields* (Gen. Albuquerque 1992) to be published
6. Date M *J. Phys. Soc. Jpn.* **39** 892 (1975)
7. Yamagishi A, Date M *Physica B* **155** 91 (1989)
8. Date M *IEEE Trans. Magn.* **MAG-12** 1024 (1976)
9. Motokawa M, Kuroda S, Date M *J. Appl. Phys.* **50** 7762 (1979)
10. Date M, et al. *J. Magn. Magn. Mater.* **15–18** 1559 (1980)
11. Date M, et al. *J. Magn. Magn. Mater.* **31–34** 140 (1983)
12. Date M, et al. *J. Magn. Magn. Mater.* **54–57** 627 (1986)
13. Date M *Physica B* **155** 119 (1989)
14. Date M *J. Magn. Magn. Mater.* **90–91** 1 (1990)
15. Date M *Physica B* **164** 108 (1990)
16. Date M *J. Magn. Magn. Mater.* **104–107** 2105 (1992)
17. Date M, et al. *J. Appl. Phys. Ser. 8* **195** (1993)
18. King A R, et al. *Phys. Rev.* **47** 117 (1981)
19. Date M, Sakakibara T, Sugiyama K *High Field Magnetism* (Amsterdam: North-Holland, 1983) p. 41
20. Haseda T et al. *Physica B* **108** 841 (1981)
21. Date M *High Field Magnetism* (Amsterdam: North-Holland, 1989)
22. Katsumata K et al. *Phys. Rev. Lett.* **63** 86 (1989)
23. Date M, Kindo K *Phys. Rev. Lett.* **65** 1659 (1990)
24. Date M, Motokawa M *Phys. Rev. Lett.* **16** 1111 (1966)
25. Morin D, et al. *J. Magn. Magn. Mater.* **81** 247 (1989)
26. Yamagishi A, et al. *J. Magn. Magn. Mater.* **90–91** 51 (1990)
27. Kuroda T, et al. *Physica B* **186–188** 396 (1993)
28. De Visser A, et al. *Solid State Commun.* **64** 527 (1987)
29. Sugiyama K, et al. *J. Phys. Soc. Jpn.* **59** 3331 (1990)
30. Sugiyama K, et al. *J. Phys. Soc. Jpn.* **57** 3946 (1988)
31. Tajima Y, et al. *Phys. Rev. B* **37** 7956 (1988)
32. Katsui A, Hidaka Y, Ohtuku H *Jpn. J. Appl. Phys.* **26** L 1521 (1987)
33. Hidaka Y, et al. *J. Phys. Soc. Jpn.* **60** 1185 (1991)
34. Hidaka Y, et al. *J. Phys. Soc. Jpn.* **60** 1185 (1991)
35. Kakeshia T, et al. *Trans. Jpn. Inst. Met.* **24** 748 (1983)
36. Hashimoto Y, et al. *Phys. Rev. Lett.* **72** 1922 (1994)
37. Uyeda C, Yamagishi A, Date M *J. Phys. Soc. Jpn.* **57** 3954 (1988)
38. Langevin P *Radium* **7** 249 (1910)
39. Yamagishi A, Nagao E, Date M J. Phys. Soc. Jpn. **53** 928 (1984)
40. Yamagishi A, et al. *J. Phys. Soc. Jpn.* **58** 2280 (1989)
41. Date M *Physica B* to be published
42. Hofstadter D R *Phys. Rev. B* **14** 2239 (1976)

PACS numbers: 43.35.Lq

Acoustic properties of glasses and polycrystals at very low temperatures

F Pobell

The properties of amorphous dielectrics at very low temperatures have universal character irrespective of their nature. They are substantially different from properties of dielectrics in crystalline state: firstly, because of the thermal capacity c and its temperature dependence [$c \propto T$ (Fig. 1) for amorphous dielectrics, but $c \propto T^3$ for crystalline dielectrics]; and secondly, because of the temperature dependence of sound velocity and attenuation.

The first effect is due to additional excitations contributing also to phonon scattering. This is the reason for essentially smaller thermal conductivity in the glass state and for the different dependence of the velocity and attenuation of sound.

The low-temperature properties have been explained in terms of two-level-systems tunnelling models, which assume that atoms or groups of atoms have more than one site in a disordered lattice and that these sites are separated by energy barriers (Fig. 2). In the simplest version of the model, only the tunnelling between the ground states of a double-well potential is considered. Because of the disorder in system, it is assumed that there is a wide range of tunnelling energies, leading to a constant density of tunnelling states, and very wide range of relaxation times. Note that they were observed experimentally to vary for 10^{-9} s to 10^{6} s.

As noted in classical studies [1, 2], the main contribution to heat capacity provide states with energy difference not exceeding T. Moreover, assuming independence of density of states on energy, one obtains a linear dependence for heat capacity. This is observed experimentally.

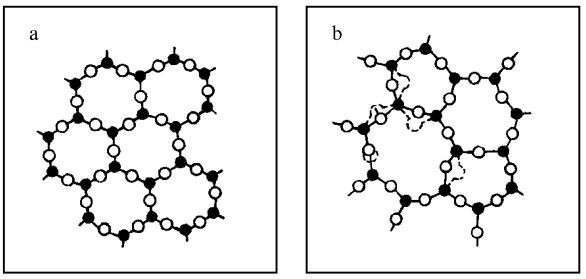

Figure 2. Schematic two-dimensional representation of SiO_2 .

Let us consider this model as applied to acoustic waves in glasses (Fig. 3). The temperature dependence of the velocity of sound must a have peak and fall logarithmically around it; the slope of the temperature curve to the right of the maximum is $\sim 1/2$ of the slope on the left. Also, within the tunnelling model one can show that the width of the plateau in Fig. 3b is correlated to the analogous curve for the sound velocity. These properties are due to wide energetic zones in tunnelling states. Model results agree well with experiment. The slope of the curve may also help to estimate the density of states.

The situation in polycrystals is not as obvious as for dielectric glasses. In this case low-energy excitations, due to defects and impurities, as expected, must have a discrete energy spectrum. And this, in its turn, must modify the logarithmic dependence of sound velocity near the maximum. Also in conductors there is the problem of how electrons interact with the tunnelling system. To resolve this problem, a series of experiments were carried out [3]. The materials used were: glass (SiO_2), polycrystalline super-

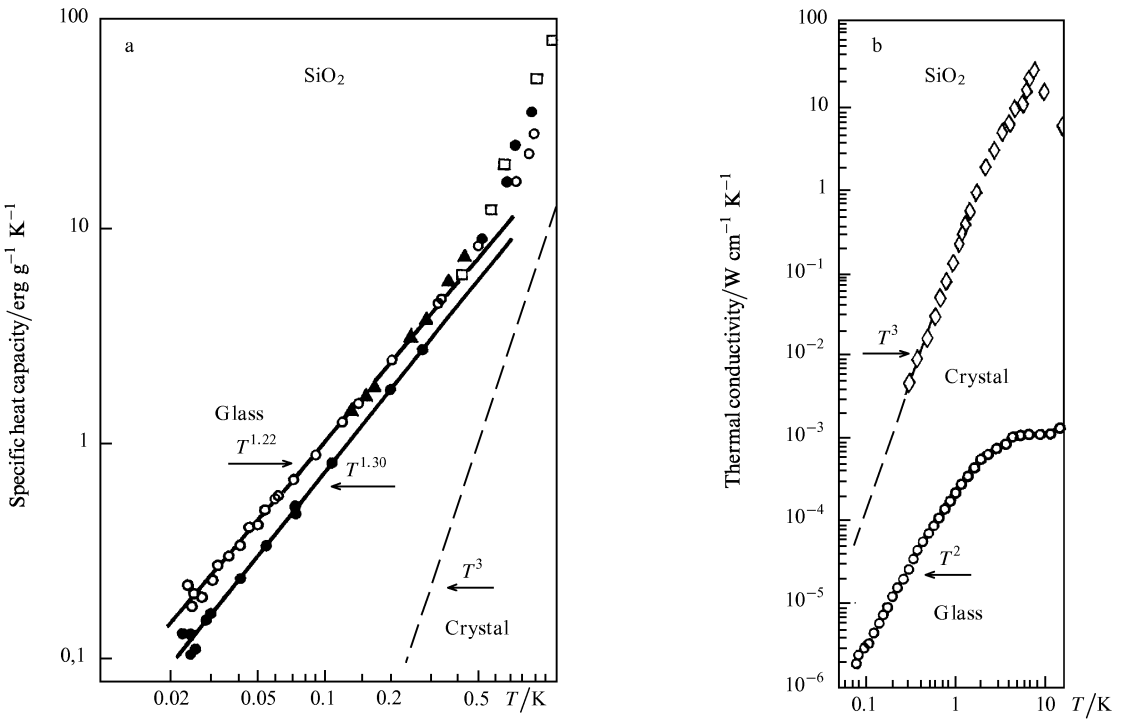

Figure 1. Temperature dependence for the heat capacity of glass (SiO_2) at various OH^- concentrations.

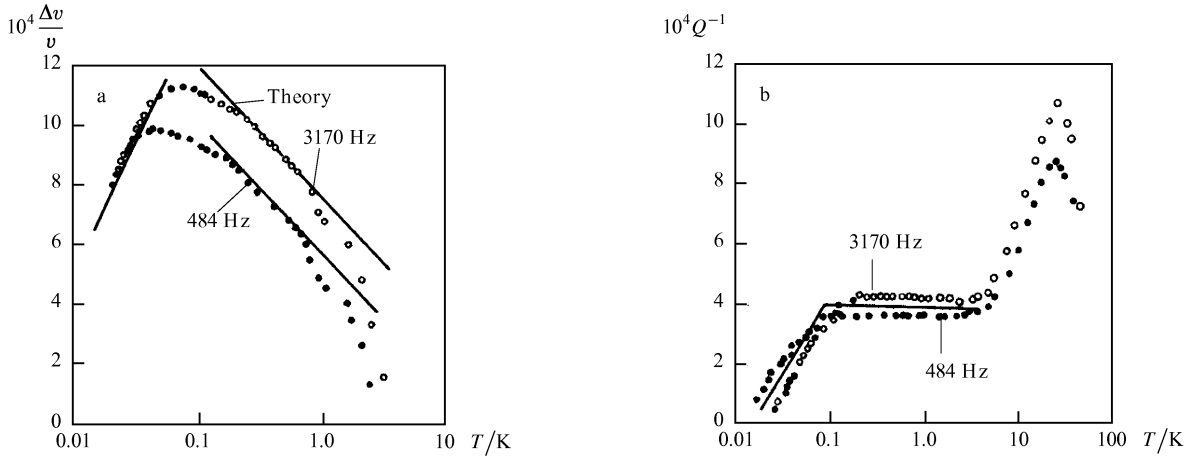

Figure 3. Sound velocity (a) and attenuation (b) in SiO_2 for two different frequencies.

conductors (Nb, NbTi, Al), and polycrystalline normal conductors (Ag, Cu, and Pt). Measurements were performed by the vibrating wire technique in the frequency range 100 Hz–8 kHz and at temperatures from 0.04 mK to 1 K.

The results of these experiments are given in Figs 4–8. They show that polycrystalline superconductors behave like dielectric glasses. Even the dependence of the sound velocity on the amplitude of the acoustic wave is the same, on neglecting heating effects. The analogy is observed also in the temperature dependence of sound attenuation (Fig. 3b). Another clear piece of experimental evidence of analogous dependence of energy on relaxation time is the structure of the plateau, depending on frequency. In accordance with the tunnelling model, this law gives a $\omega^{1/3}$ dependence for the temperature (Fig. 8).

So the study of amorphous superconductors, at temperatures well below the critical temperature, showed that their acoustic properties agree well with the tunnelling model. As noted above, the interaction between conduction electrons and tunnelling systems essentially complicates the problem [4], as indicated by the theory of Kagan and Prokof'ev. But low-frequency acoustic properties appeared

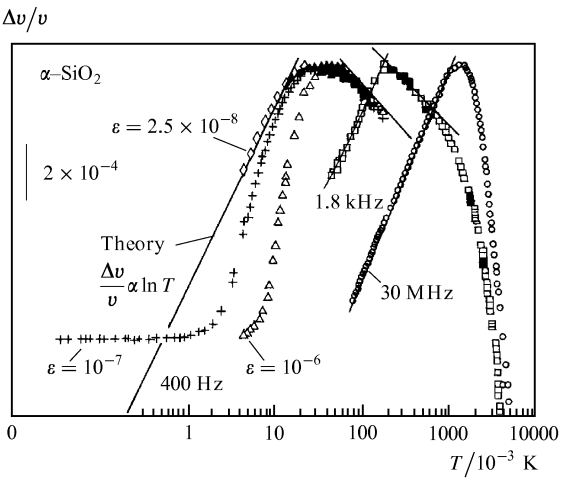

Figure 4. Temperature dependence of the relative variation of sound velocity in SiO_2 at various intensities of acoustic waves.

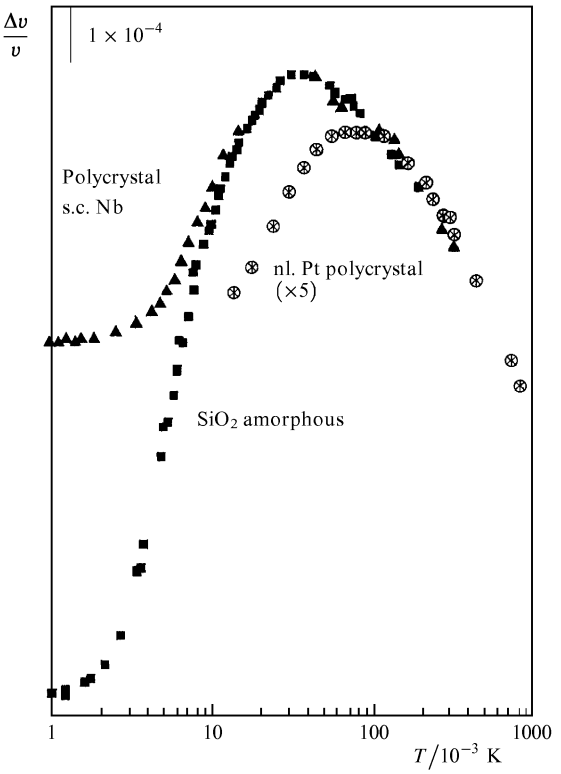

Figure 5. Relative variation of sound velocity in samples of SiO_2 and polycrystals of Nb and Pt.

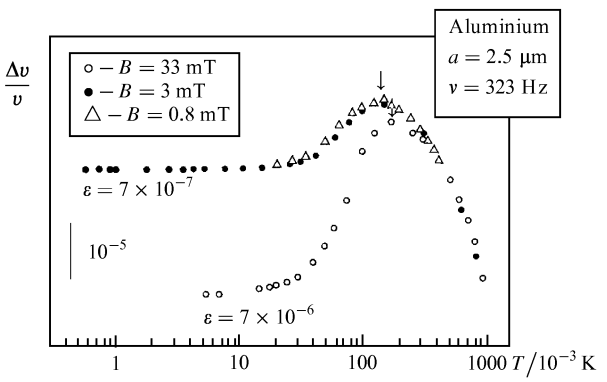

Figure 6. Sound velocity versus acoustic wave intensity ε in Al.

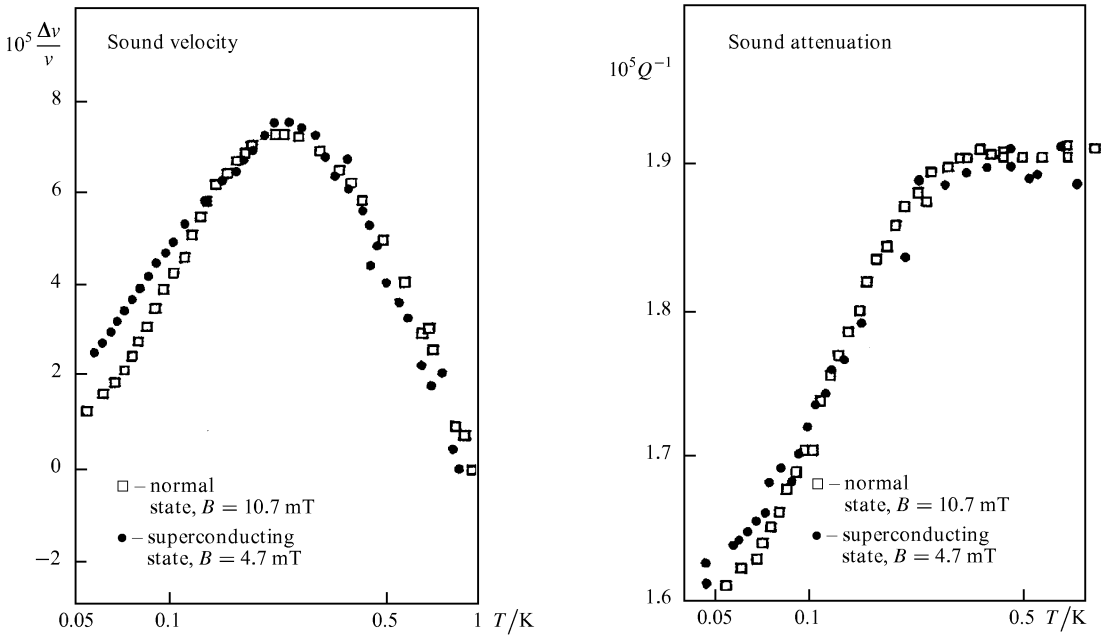

Figure 7. Al in normal and superconducting states.

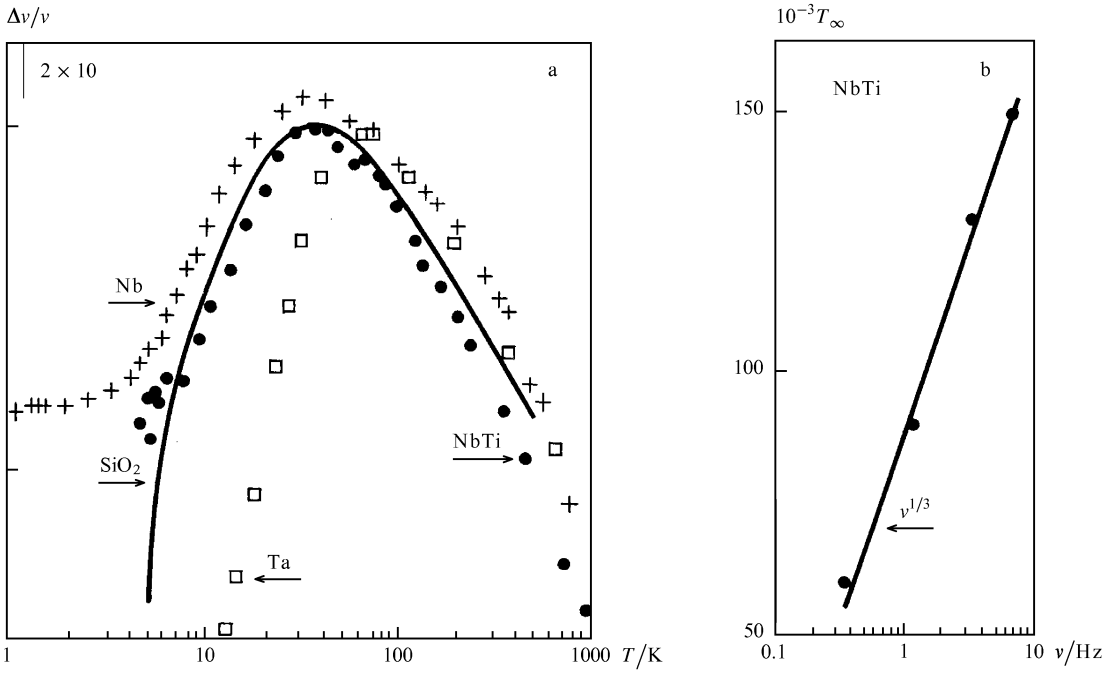

Figure 8. (a) Relative variation of sound velocity in SiO_2, Ta, Nb and NbTi; (b) Frequency dependence of the onset temperature of the plateau on the sound attenuation of NbTi.

to be analogous for SiO_2 and polycrystals. Even a decrease of impurity concentration in Ag from 100 ppm to 1 ppm had only a small influence on the velocity and attenuation of sound.

But at low temperatures $T < 10$ mK and frequencies near 400 Hz the experimental data disagree with theory. Disagreement is in the shift of the maximum, depending on the amplitude of the acoustic wave, and in saturation at low temperatures. Note that the shift of the maximum is an effect quite opposite to what could be expected, if one assumes sample heating. The influence of acoustic wave intensity was observed at energies near $k_B T$. Possibly this is due to a change of the number of tunnelling states under the influence of phonons. Below the plateau attenuation decreases linearly, but not as $Q^{-1} \propto T^3$, as was expected.

The results of studying acoustic properties of different polycrystalline superconductors and conductors indicate that their behaviour is very similar to that of glass in a wide range of temperatures. Is this similarity of quantitative or of qualitative nature?

References

1. Anderson P W, Halperin B I, Varma C M *Philos. Mag.* **25** 1 (1972)
2. Philips W A *J. Low Temp. Phys.* **7** 351 (1972)
3. Esquinazi P, Koenig R, Pobell F *Z. Phys. B* **87** 305 (1992)
4. Kagan Y M, Prokof'ev N V *Zh. Eksp. Teor. Fiz.* **97** 1698 (1990)

PACS numbers: 67.65.+z

The Kapitza leap on the boundary of superfluid ^{4}He and atomic hydrogen gas

J T M Walraven

The 'Kapitza leap' effect was discovered in 1941 [1] and explained, on the basis of acoustic disbalance theory, by I M Khalatnikov in 1952 [2]. The effect consists of the existence of a finite temperature difference between superfluid helium, which has infinite thermal conductivity, and a solid; or, generally, between any two substances with high thermal conductivity. Since then this effect has often played an important role in the understanding of many fundamental and applied problems of low-temperature physics and cryogenics.

Here we consider the Kapitza leap between atomic hydrogen gas $H^{\downarrow}$, which is in spin-polarised state, and a film of superfluid ^{4}He on the walls of the experimental cell. Insights of nature and quantitative estimation for such systems are of great importance for the practical realisation of temperature and density parameters for Bose condensation in atomic hydrogen, i.e. for the creation of a new superfluid Bose system.

It is known that the value of the Bose-condensation temperature in a Bose gas can be computed from the formula

$$k_B T_c = 3.31 \frac{\hbar^2 n^{2/3}}{m} ,$$

where n is the density of the system. For $n = 10^{19}$ cm^{-3} we obtain $T_c = 0.1$ K. Therefore, to reach Bose condensation, one needs low temperatures or high densities. In the latter case three-particle recombination in a volume and on the surface of the film prevents the system reaching Bose-condensation. The theory of this process was developed by Yu M Kagan, Y V Shlyapnikov, and I A Vartanyants [3]. According to it, dipole–dipole interaction of electronic spins in the case of ternary collisions causes depolarisation of atomic hydrogen and, consequently, its recombination to H_2 molecules. It is natural that velocities of volumetric and surface recombinations are proportional to n^3 and strongly increase at high densities. At smaller densities, when temperature is substantially less than the binding energy of hydrogen $\varepsilon_0 \sim 1$ K, the prevailing channel in the surface potential well becomes a three-particle surface recombination. Its rate is proportional to n_s^3,

$$n_s \sim \exp(\varepsilon_0/T)\, \overline{s(T, \theta)} ,$$

where n_s is surface density, and s is the adhesion coefficient. To suppress this relaxation channel, it is necessary to decrease the volumetric density of hydrogen drastically. In this case one needs very low temperatures for reaching Bose condensation. But here the Kapitza leap intervenes, tending to warm up the system on the interaction of particles with surface: $\dot{Q} = R_K \Delta T$, where ΔT is the difference of system and wall temperatures, $\dot{Q}$ is the heat flow per unit time. On the boundary of atomic hydrogen and superfluid helium the inverse Kapitza heat resistance is given as

$$R_K^{-1} \propto n\bar{v}\overline{s(T, \theta)} ,$$

i.e. proportional to the average thermal velocity of the gas $\bar{v} \propto \sqrt{T}$, and to the adhesion coefficient $s(T, \theta)$. So decrease of adhesion coefficient leads to suppression of the three-particle surface recombination but, simultaneously, to warming up of the system. Hence it follows that it is important to know how s depends on temperature and angle, if one wants to find optimal parameters of Bose condensation. According to the theory of Kagan–Shlyapnikov, the function $s(T, \theta)$ is determined mainly by the de Broglie wavelength and conservation laws for energy and momentum at scattering. Note that there are three possible variants for interaction of a hydrogen atom with the surface: purely elastic, leading to mirror reflection; direct inelastic interaction with surface, accompanied by emission of a surface wave (ripplone); capture of a particle by surface potential well, simultaneous emission of ripplone, leaving potential well and joining ripplone. The third variant gives purely diffuse scattering and determines the adhesion coefficient.

In a series of experiments [4] $s(T, \theta)$ was studied in a wide range of temperatures and angles. At the first stage a thin and long capillary with length L and diameter a was used. We created a pressure difference across the capillary ends and observed the Knudsen flow ($l \gg a$) of atomic hydrogen. We also measured the so-called Klausing factor K (see Fig. 1), equal to the probability of penetrating through the capillary. At purely mirror reflection $K = 1$, so the adhesion coefficient is equal to zero. At diffuse reflection

$$K = \frac{8}{3}\frac{a}{L} \ll 1 \quad \text{and} \quad s \to 1 .$$

The experiment with thin capillaries showed that the scattering is mainly of mirror type, and the adhesion coefficient depends on temperature linearly, being much less than 1. This result was later confirmed in 'atomic optic', experiments where we used a parabolic mirror for focusing particle rays. The distance between the mirror and the receiving detector was variable. When the detector was in focus, it counted a relative number of mirror-scattered particles. Shifting the detector from a focus, one could

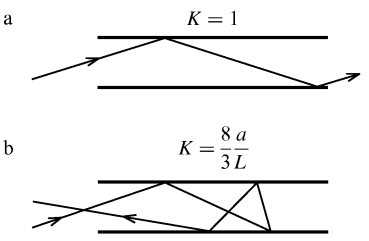

Figure 1. (a) mirror reflection of H atoms in thin capillary; (b) diffuse reflection of H atoms.

count diffusely scattered particles. In other words, the device measured angular dependence of the reflection coefficient. The results showed that 80% of particles are scattered through mirror reflection, so that $s \leqslant 0.2$; this agrees with earlier capillary experiments. In conclusion it should once more be emphasised that detailed study of the adhesion coefficient $s(T, \theta)$ and Kapitza heat resistance R_K is very important for experimental attainment of temperatures necessary for Bose condensation in spin-polarised atomic hydrogen.

References

1. Kapitza P L *Zh. Eksp. Teor. Fiz.* **11** 1 (1941)
2. Khalatnikov I M *Zh. Eksp. Teor. Fiz.* **22** 687 (1952)
3. Kagan Y M, Vartanyan I A, Shlyapnikov G V *Zh. Eksp. Teor. Fiz.* **81** 1113 (1981)
4. Berkhout J J, Wolterrs E J, van Roijen R, Walraven J T M *Phys. Rev. Lett.* **57** 2387 (1986)

PACS numbers: 67.57.De; 67.57.Np

Excitations in superfluid ^{3}He †

G R Pickett

The excitation gas in superfluid ^{3}He is unique in that it is one of the few in nature in which an entire assembly of particles with non-Newtonian dynamics is completely accessible to experiment. There are similar ensembles of excitations found in other systems but invariably in solid materials entrapped in a rigid lattice. In superfluid ^{3}He the excitation gas moves in the background medium of the superfluid condensate alone. For most purposes the condensate can be considered as a 'mechanical vacuum' and the independent dynamics of the excitations can be studied by mechanical methods. This is most easily done at very low temperatures where the low excitation density means that the excitations collide only rarely and the motion is wholly ballistic over the length scale of a typical experiment.

The unique behaviour of the excitations arises from the particular form of the dispersion curve which is quite different from the Newtonian parabola, in that the energy minimum falls not at zero momentum but at the Fermi momentum where there is also an energy gap, Δ. This shape gives rise to two different types of excitation: quasiparticles which have group velocity and momentum parallel and quasiholes which have group velocity and momentum opposed.

Because of the energy gap to the minimum excitation energy at low temperatures the expression for the excitation density is dominated by the gap Boltzmann factor $\exp(-\Delta/kT)$. At the lowest temperatures we can currently reach (around 100 μK at zero pressure) this density is so small that the mean free paths become of the order of kilometres, orders of magnitude longer than any experimental dimension. This allows us to carry out experiments with noninteracting beams of excitations.

The mechanical behaviour of the excitation gas is largely governed by the phenomenon of Andreev reflection. This arises from the fact that near the minimum in the dispersion curve an excitation may have its group velocity reversed for a negligible change in momentum. This behaviour comes into play when a quasiparticle (quasihole) incident on a region of increasing gap is retro-reflected as a quasihole (quasiparticle). This process was first discussed by Andreev in the context of electron reflection at a normal–superconducting interface, where the excitation energy is reflected but the electric current continues into the superconductor as a Cooper pair. In the superfluid ^{3}He context such reflection processes have a very strong influence on the dynamical properties, since they permit an excitation to be reflected with virtually no change of momentum.

When we observe the excitation dispersion curve in a moving frame, it becomes distorted. This is one of the most interesting aspects of this system. The usual $E = p^2/2m$ parabola for a Newtonian particle is not distorted but simply translated since there is no absolute rest frame. However, our excitations are not free particles obeying Einsteinian relativity but are tied to the condensate and thus have a preferred rest frame. The result is that as we move relative to the liquid, excitations with momenta approaching are seen to have increased energies and those with momenta receding decreased energies. Thus the effective gap for approaching excitations increases and that for receding excitations decreases.

Our experiments are performed largely with vibrating wire resonators (VWRs). Here a wire is oscillated mechanically in the liquid and the behaviour of the excitation gas inferred from the damping. Once we are well below the superfluid transition temperature the excitation density is dominated by the $\exp(-\Delta/kT)$ factor. We would expect the damping to reflect this, which indeed it does but with a value several orders of magnitude larger than would be expected from simple kinetic gas arguments. What we have neglected is the fact that the quasiparticle and quasihole excitations interact with the moving wire in different ways. The distortion of the dispersion curve in the (moving) frame of the wire resonator means that on the leading side of the wire a large fraction of the quasiholes are Andreev reflected, which means they exchange no momentum with the wire and may be ignored. Similarly on the trailing side of the wire a large fraction of the quasiparticles are also Andreev reflected. This sets up an asymmetry since the normal reflection processes, the only ones which interchange momentum on the wire, are largely from quasiparticles on the front side and quasiholes on the rear side. However, a quasiparticle striking the wire pushes it whereas a quasihole pulls it. Thus the net forces on the wire from the normal process on both front and rear sides, instead of opposing each other as in a normal gas, both act in the same direction, to damp the motion. This has the effect that an extremely dilute gas of excitations can exert an extremely strong force on a moving wire and thus the excitations are very easy to detect and we can use them as probes in a number of experiments.

In recent beam experiments we have made use of the quasiparticle 'blackbody radiator'. This device consists of a box having a small hole in one face containing inside two VWRs, one to act as thermometer and one as a heater. These devices are extremely sensitive and show a linear calibration in applied power over 7 orders of magnitude. When heated the radiator puts out a thermal beam of excitations through the hole at a temperature corresponding

† The text of this article (in Russian) and those by M Krusius, D M Lee, and O V Lounasmaa have bee published in full in the Russian journal *Priroda* issue 4, 1994.

to the temperature in the box. This is the 'source' mode. Alternatively we can detect a flux of excitations incident on the hole from outside since the excitation density in the box builds up until equilibrium is reached, at which point the temperature inside is a very accurate measure of the energy flux incident on the hole. The blackbody radiator may thus act either as source or as detector.

We have only just begun to exploit this device but the most significant use so far has been to make a direct observation of Andreev reflection in superfluid ^{3}He. A blackbody radiator puts out a beam incident on what is essentially a flat paddle. When the paddle is stationary the excitations are normally reflected and lost in the bulk liquid. But when the paddle moves a superfluid backflow is set up which distorts the dispersion curve of the incident beam and leads to Andreev reflection of a fraction of the excitations. When this occurs, the Andreev reflected particles are retro-reflected back into the box, thereby increasing the excitation density inside, which we can easily measure.

In the future we hope to make direct observations of the reflection of excitations at an A–B phase interface (where there is a jump in the gap) with blackbody radiators on both sides of a static A–B boundary stabilised by a magnetic field. Since we do not yet know how a blackbody radiator will operate in the A-phase, we have a further variant of this experiment where the beam from a blackbody radiator is incident on a small region of A-phase stabilised by a high field generated by a small solenoid. The retro-reflection of excitation excitations by the phase boundary should be detectable in the source radiator as an increase in excitation density. This configuration has the advantage that only one radiator is needed which can then operate in the B-phase.

Looking further ahead, we are considering the use of quasiparticle excitation beams to probe the structure of the vortex lattice in rotating systems in collaboration with the Helsinki group. The flow field associated with each vortex introduces a large Andreev reflection aspect into the transmission of excitations through such a lattice and the interaction should be very strong.

Ultralow power dissipation measurements are becoming a possibility with the blackbody radiator. A copper box with a 0.3 mm diameter hole can resolve powers of the order of 1 fW. This could be improved by some orders of magnitude by a corresponding decrease in the area of the hole. We should be able to make these radiators sensitive enough to be used as particle detectors.

The low temperature regime is likely to provide a number of interesting surprises for some time to come since the excitation gas has such unusual properties that many more counter-intuitive phenomena will surely come to light.